University of Zurich[UZH]

Glacier-induced Tsunamis: A wood anatomical reconstruction in West Greenland

GEO 511 Master's Thesis

Author
Danijar Manser
13-711-197

Supervised by
Dr. Holger Gärtner (holger.gaertner@wsl.ch)

Faculty representative
Prof. Dr. Andreas Vieli

29.04.2019
Department of Geography, University of Zurich

University of Zurich[UZH]

GEO 511 Master's Thesis

Glacier-induced Tsunamis

A wood anatomical reconstruction in West Greenland

Author
Danijar Manser
danijar.manser@uzh.ch
13-711-197

Supervisor
Dr. Holger Gärtner
Eidg. Forschungsanstalt WSL
Zürcherstrasse 111
8903 Birmensdorf
holger.gaertner@wsl.ch

Supervisor & Faculty Representative
Prof. Dr. Andreas Vieli
Department of Geography
Andreas.vieli@geo.uzh.ch

30th April 2019
Department of Geography, University of Zürich

Abstract

In polar regions, the processes of iceberg calving from marine-terminating outlet glaciers possess the potential to generate tsunamis of considerable size. These tsunamis can pose a significant threat to human populations and infrastructure in coastal zones. The detectable increase in the retreat, flow and calving rate of many glaciers in West Greenland is a consequence of recent global warming. Very little is known about the frequency and magnitude of glacier-induced tsunamis, yet erosion and deposition of material in affected coastal areas may influence vegetation. Consequently, Arctic shrubs represent a potential archive of past tsunami events since the physical disturbances caused by glacier-induced tsunamis should be evident within their growth and cell structure. In this regard, disentangling the effects of the local climate as a growth limiting factor and the mechanical disturbances on Arctic shrubs is essential for reconstructing past tsunami events. Ring width and anatomical measurements spanning the last four decades are presented from a cohort of disturbed and undisturbed *Betula nana* shrubs located near the calving outlet glacier Eqip Sermia, West Greenland. A standard reference ring width chronology for *Betula nana* was developed using micro sections as a base for detecting tsunami-induced disturbances, also enabling the identification of anatomical variations. Results provide insights into the growth limiting responses of shrubs affected by glacier-induced tsunamis, visible in form of narrower rings in years with increased tsunami activity. A documented tsunami event in 2013 was used to reconstruct 6 further events. Glacier-induced tsunamis likely increased in magnitude, as the spatial reach of recent tsunamis was larger than events occurring before 1997. However, no correlation between vessel lumen area and ring growth was found. This study provides the basis for improving our understanding of how glacier-induced tsunamis affect the growth of Arctic shrubs and the applicability of this method for reconstructing past tsunami events.

Table of content

List of Figures

List of Tables

1 Introduction

1.1 Context

Modern increases in global temperature are mainly driven by the rise in greenhouse gases, with Arctic regions and Arctic Tundra ecosystems being particularly vulnerable to these changes (Box et al. 2019). The Intergovernmental Panel on Climate Change (IPCC) defines climate change as statistical changes in the mean or variability of the physical state of the climate over a period of a decade or longer, whilst a changed state of the atmosphere is induced by human activities, rather than natural climate variability (IPCC 2014). Notable changes of the global average surface temperature (land and ocean combined) are defined as global warming and identified by comparing temperature averages from preindustrial times (years 1850-1900) to modern temperatures observed over a period of 30 years (Allen et al. 2018).

The IPCC estimates that a mean global surface temperature increase of 1°C (between 0.8 °C and 1.2 °C) occurred between preindustrial times and a modern reference period (IPCC 2018). Global air and ocean surface temperatures are currently increasing at a rate of 0.2 °C per decade (Allen et al. 2018). Box et al. (2019) suggest that Arctic temperatures are rising faster than the global average as for the period between 1971 and 2017, a temperature increase of 2.7 °C in Arctic regions was noted, a rate of 2.4 times the average increase of the northern hemisphere.

In response to rising global surface temperature, a near worldwide melting of glaciers and land ice masses has been observed, including the thawing permafrost in high latitude regions (IPCC 2014). These changes in global surface temperature drive global glacier retreat, sea level rise, changes in seasonal water availability and increase hazards to human society (Marzeion et al. 2014).

Between 2002-2011 mass loss of the Greenland Ice Sheet (GIS) has increased by 181 Gt yr-1 relative to that of the 1992-2001 period (IPCC 2013). Increased summer temperatures and subsequent increased surface melt of the GIS, cause an increased flow towards the ice margins and the outlet glaciers of the ice sheet (Zwally et al. 2002).

Tidewater glaciers (also marine-terminating outlet glaciers) transport ice mass directly from the land to the sea through frontal ablation (iceberg calving and submarine melt) (Schild et al. 2018). Greenland's tidewater glaciers are responsible for one third to half of the total annual mass loss of the ice sheet through calving and submarine melt (Benn et al. 2017; Enderlin et al. 2014; Moon et al. 2015; Rignot et al. 2008). The increasing frontal ablation of tidewater glaciers correlates positively with air and sea water temperature increases, making Greenland's marine-terminating outlet glaciers particularly sensitive to atmospheric and oceanic temperature increases (Benn et al. 2017). Submarine melting plays a significant role in frontal ablation of tidewater glaciers even though it is hard to determine its contribution to frontal ablation compared to glacier calving (Schild et al. 2018; Benn et al. 2017). Rignot et al. (2010) stress that frontal calving is clearly connected to submarine melting as it influences calving mechanisms below water surface (Rignot et al. 2010).

Glaciers possess the potential to cause large tsunami waves during the calving process (Fritz et al. 2003). Two glacial processes can cause a tsunami waves; glacial calving of marine-terminating outlet glaciers

or the rotation of icebergs originating from such a glacier (Macayeal et al. 2011; Lüthi & Vieli 2016). Large calving events accompany the creation of icebergs and are a common phenomenon in polar regions as a full frontal collapse of the glacier tongue, subaquatic calving or a partial break-off (Lüthi & Vieli 2016). In narrow fjords and bays, waves can be intensified due to the shallower bathymetry and confined outlet geometry possessing a high destructive potential, causing erosion along the fjords and destruction of infrastructure in some extreme cases (Lüthi & Vieli 2016). Icebergs may also generate tsunamis through tilting, rotation or breaking apart (Long et al. 2015) and their orientation in the water is crucial for their stability which may cause capsizing in order to become stable in the water (Macayeal et al. 2011). Through the rolling movement of the iceberg, large quantities of water are displaced and large waves are put in motion (Levermann 2011). Glacier-induced tsunamis are a common occurrence in polar regions. Major events have been described in Greenland (Long et al. 2015; Amundson et al. 2010) and in Antarctica where they are known to intensify the collapse of Antarctic shelf ice as a self-stimulating, chain-reacting process (Macayeal et al. 2011; Macayeal et al. 2009).

1.2 State of the art

Multiple studies described the extent and dynamics of tsunamis in polar coastal regions looking both at calving-induced and iceberg-induced tsunamis. However, they lack focus on the reconstruction of past tsunami events (e.g. Levermann 2011; Macayeal et al. 2011; Macayeal et al. 2009). A possible method for reconstructing historical tsunamis in West Greenland, triggered by glacial ablation processes is introduced by Long et al. (2015). The occurrence of a likely iceberg-induced tsunami has been dated to approximately 6000 years ago using coastal lake sediments to reconstruct the tsunami activity (Long et al. 2015). Other observations focused more on the calving-events of West Greenland's outlet glaciers which have the potential to trigger tsunamis (Amundson et al. 2008; Lüthi & Vieli 2016).

Lake deposits have the potential to reconstruct historical tsunamis, as first applications of a dendrochronological approach to reconstruct tsunami events have been conducted by Buchwal et al. (2015) for application in more recent time periods. They used *Salix glauca* to reconstruct a tsunami event in West Greenland by the analysis of ring width measurements on four samples as well as wood anatomical indices of physical disturbances (Buchwal et al. 2015). However, the analysed tsunami event occurring in 2000 was landslide-induced and dendrochronological reconstructions of glacier-induced tsunamis are still lacking. Due to the small sample size involved in the study of Buchwal et al. (2015), the applicability of dendrochronological based tsunami reconstructions remains equivocal.

This thesis will make a contribution to linking glacier-induced tsunamis effects to shrub vegetation, using a dendrochronological approach. Tsunami triggered by glacier calving in West Greenland are still poorly understood as they pose a threat to coastal regions, causing erosion to soil and vegetation (Lüthi et al. 2016). Growth limiting effects on the shrub vegetation by tsunamis occurring in specific years were not part of the analysis of Buchwal et al. (2015), only average, minimum and maximum ring width were included. How tsunamis may limit the growth response of shrubs is still not clear as there is a lack of evidence as to how glacier-induced tsunamis affect the annual (ring) growth of dwarf shrubs. In

particular, the exact and labour-intensive crossdating, as well as the potential for missing rings in Arctic shrub growth can pose a challenge to the accuracy of results (Myers-Smith et al. 2015; Buchwal et al. 2015). *Betula nana* has the potential to become a possible archive for the reconstruction of past tsunamis that had a growth limiting effect on the plant growth. This will provide a better understanding of the potential risks and hazards that are posed by glacier-induced tsunamis to West Greenland's coastal regions and potentially provide better understanding of historical changes in glacier dynamics as these are linked to glacier-induced tsunami activity.

1.3 Aims and research questions

The primary goal of this thesis is to ascertain whether evidence of glacier-induced tsunamis is preserved in the growth pattern of dwarf shrubs located in West Greenland. This be achieved through ring width measurement in *Betula nana* and measurements of vessel lumen area on a wood anatomical level. The following six research questions were used to formulate hypotheses to guide through the investigations of glacier-induced tsunami influence on the growth of Arctic shrubs.

1) «Do glacier-induced tsunamis affect the growth of dwarf shrubs and is this visible in the ring structure?»

Glacier-induced tsunamis limit the growth of the sampled dwarf shrubs (*Betula nana)* and growth limitations are visible in form of smaller growth rings compared to a reference chronology of the same area.

2) «Are measurable differences or growth limitations present in annual vessel lumen area (VLA) and how do they correlate with the measured ring width (RW) of the shrubs?»

Annual differences in vessel lumen area are detectable and they positively correlate with plant growth.

3) «Is it possible to date past tsunami events by using the aforementioned dendrochronological approach?»

It is possible to date disturbances or growth limitations in shrubs and related these to tsunami events or years of frequent tsunami occurrence.

4) «What is the maximum inland spatial extent of tsunami influence on shrubs?»

The extent of tsunamis can be mapped and distances between affected shrubs and the edge of erosion can be measured using GIS. Shrubs growing in Z_3 and Z_2 show signs of disturbances.

5) «Is there a temporal pattern in glacier-induced tsunami frequency and how does this correspond to the frontal position of Eqip Sermia outlet glacier?»

A temporal pattern of event years is noticeable with tsunami-induced disturbances increasing in recent years. Effects of the formation of the high calving front after 2010 are evident in the disturbances.

6) «Can shrub growth be correlated to climate records of the area?»

Shrub growth correlates with climate records from the same area, such as regional temperature and precipitation records from Ilulissat.

1.4 Workflow

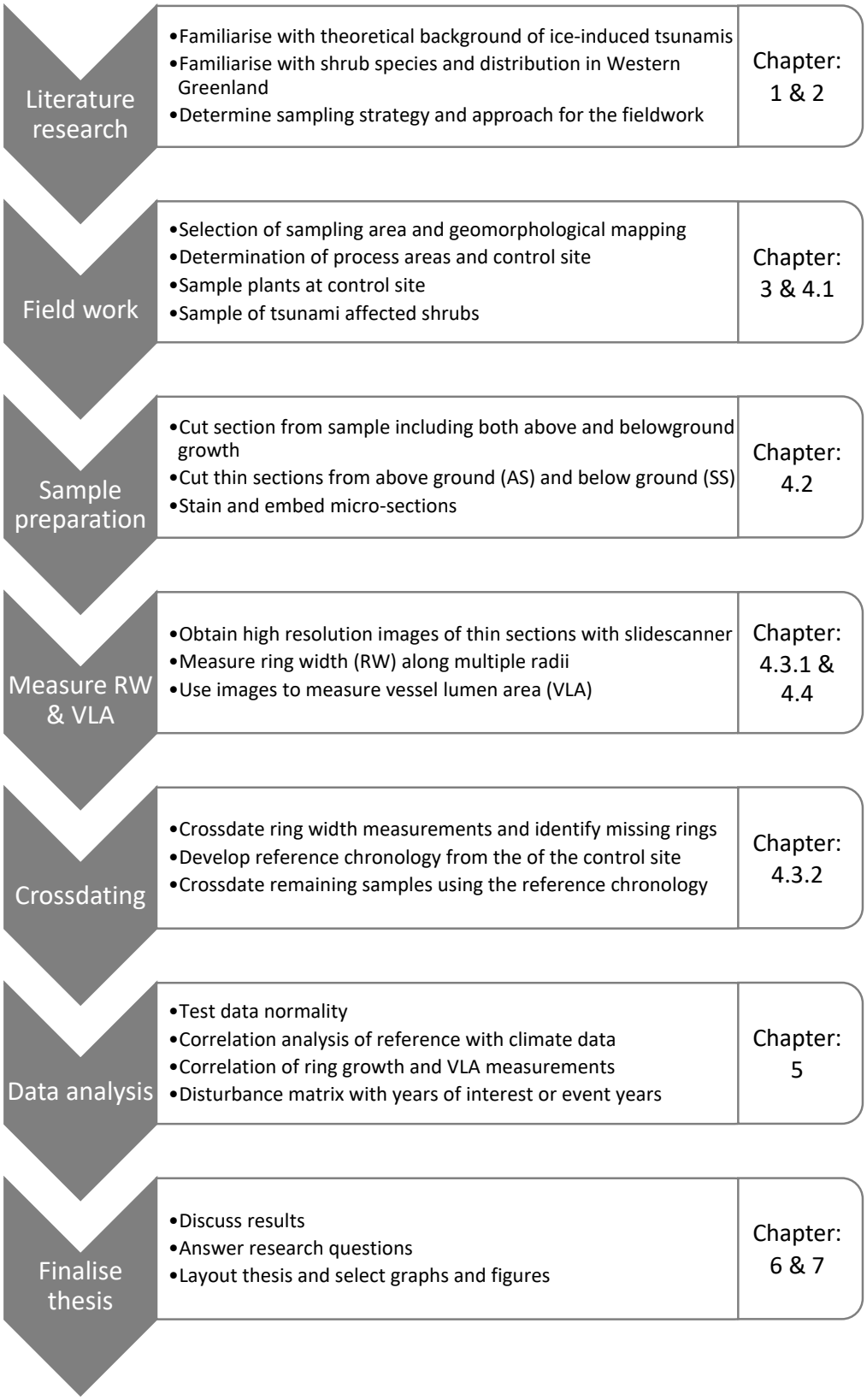

Figure 1: Workflow overview with specific descriptions of the entire working process, including the chapter of relative section.

2 Theoretical background

2.1 Marine-terminating outlet glaciers

Both solid and liquid discharge from marine-terminating outlet glaciers are responsible for about 50 % of the total mass loss of the Greenlandic ice sheet and therefore play a crucial role in calving and iceberg-generating processes (Lüthi et al. 2016). Glaciers which terminate in a waterbody can be found in many parts of the world and are often characterised by a high flow velocity at the terminus (Meier & Post 1987). Comparable to ice streams, the beds of marine-terminating glaciers lie below sea level and occur in two forms; 'grounded' where the ice sits on the glacial bed or 'floating' with a glacier tongue detached from the ground (Meier & Post 1987). For an outlet glacier terminating in a fjord or bay, a steady sea ice cover, which is also partially present during the summer, determines whether a floating terminus may be present or not, since calving processes are slowed down (Higgins 1991). Marine-terminating outlet glaciers are present in zones of differing thermal regimes (e.g. temperate, subpolar and polar), whilst the thermal regime is, to some extent, responsible for whether a floating glacier tongue is possible or not (Meier & Post 1987). Joughin et al. (2008) showed that temperate glaciers do not form floating glacier tongues, whilst polar outlet glaciers can produce floating termini of several kilometres, yet for both types, the mass loss occurs through glacial calving and submerged ice melt.

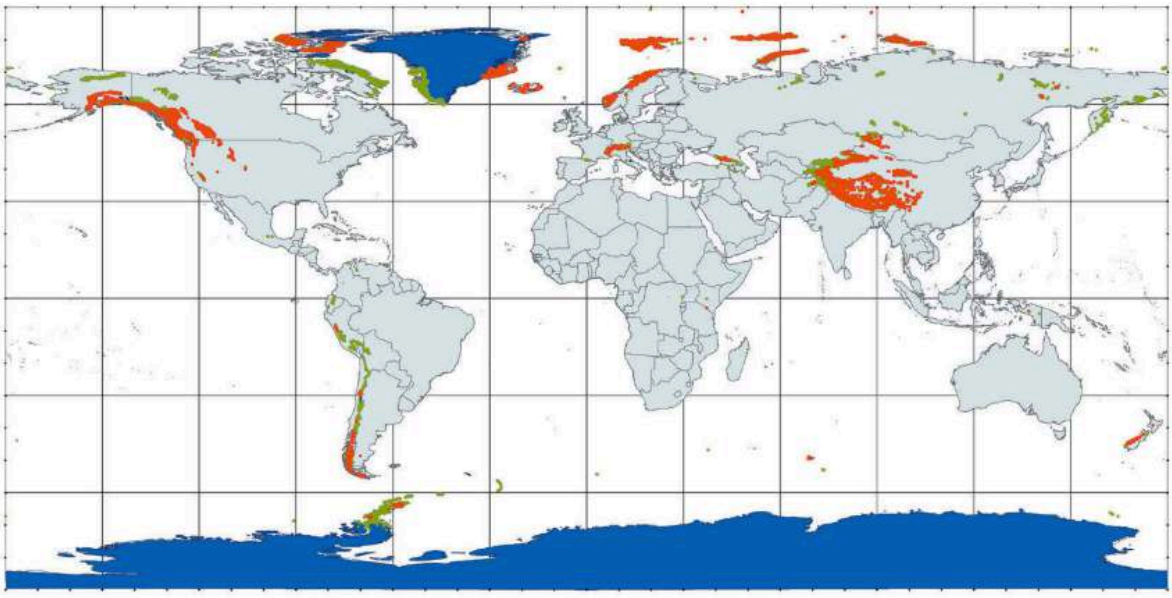

Figure 2: Global distribution of inventoried glaciers by Hoelzle et al. (2014, p. 10) *Surface land ice is indicated with blue is overlain by glacier contours of the GLIMS initiative (red) and the WGI initiative (green).*

Many studies in recent years have suggested a high sensitivity of marine-terminating outlet glaciers to environmental changes, such as rising global sea and air temperatures (Nick et al. 2009; Howat et al. 2010; McFadden et al. 2011), which affect outlet glaciers via two main mechanisms. It is suggested that increased calving and melting causes a thinning of the glacial front as a result of variations in climate and ocean conditions (Howat et al. 2010). This alters the flow dynamics and position of the calving front, and an increased availability of surface meltwater can reach the subglacial drainage system (Nick

et al. 2009; Howat et al. 2010). These mechanisms may cause increased flow velocities at the terminus and rapid changes in the frontal positions of the glaciers. Changes in the mechanisms of marine-terminating outlet glaciers are likely to continue in the future and are highly relevant since these can be expected to contribute to future sea level rise (Lüthi et al. 2016) (Figure 3).

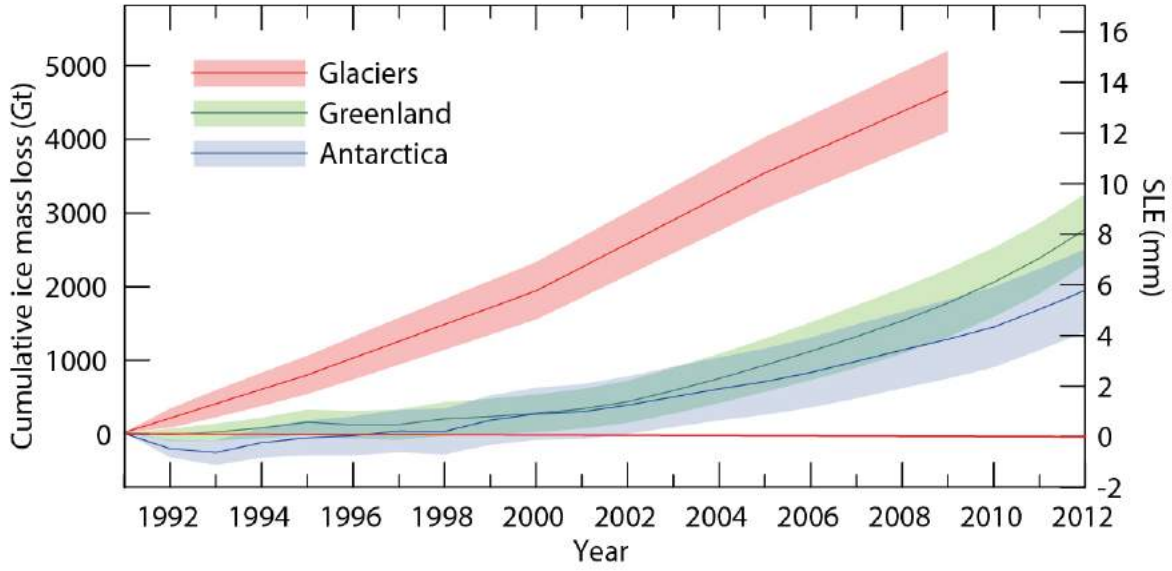

Figure 3: Cumulative ice mass loss from 1992-2012 in Gt with according sea level equivalent (SLE) in mm (Stocker et al. 2013, p. 41).

2.1.1 Calving

Calving is the mechanical loss of glacial ice, in addition to surface melt and runoff, and is a significant contributor to the total mass loss of marine-terminating outlet glaciers (Benn et al. 2007). Specifically, calving is the process whereby a quantity of ice detaches from the main glacier body at the 'calving front' via fracturing and may occur under different thermal regimes across various parts of the world (Van der Veen 2002). Marine-terminating glaciers are categorised by the properties of the proglacial waterbody in which the calving takes place (e.g. freshwater and seawater). As such, 'tidewater glaciers' are those terminating in the sea and 'freshwater glaciers' are those terminating in a proglacial lake (Benn et al. 2007). Calving is not limited to polar regions but also includes alpine environments where a suitable thermal regime exists. In the absence of a water body, dry calving can occur, a process found in arid polar regions where ice detaches from terminal ice cliffs (Benn et al. 2007).

Van der Veen (2002) distinguishes different types of calving as a function of the mechanisms responsible for ice failure.

1. Differential flow velocities at the terminus, and over-steepening of the ice cliff, can result in a subaerial launch of ice (Figure 4a).
2. Force imbalances can lead to upstream crevasses penetrating the thickness of the glacier (surface to base), resulting in the failure of large icebergs at the terminus (Figure 4b).

3. When thermal erosion (submarine melt) below the water line exceeds thermal erosion of surface melt, a horizontal undercut is the result which leads to calving of the overhanging ice (Kirkbride & Warren 1997) (Figure 4c).
4. Subaqueous calving is generated by two processes; either calving above the waterline exceeds the glacier toe below the water line and/or surface melt of the terminus exceeds the thermal erosion in the water (Benn et al. 2007). These processes lead to an accumulation of ice beneath the water surface, and as buoyant forces of this surplus ice increase (ice is less dense than the surrounding water), failure occurs, with calving ice detaching and then rising to the surface (Benn et al. 2007; Van der Veen 2002; Kirkbride & Warren 1997) (Figure 4d).

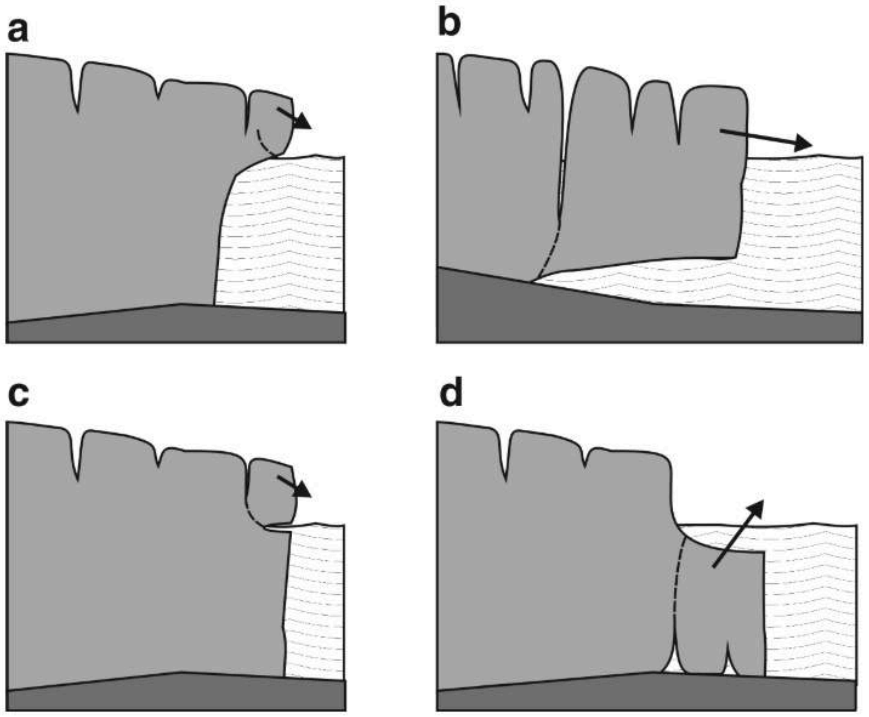

Figure 4: Four calving mechanisms responsible for iceberg production at glacier front through a) subaerial ice launch, b) failure of glacier tongue, c) failure as a result of thermal erosion at water level and d) subaqueous calving (Van der Veen 2002, p. 99).

Calving glaciers can be studied on different continents and some regions have a long history of calving studies. Alaska's tidewater glaciers have been subject to glacier studies since early on in the 20th century, for instance Columbia Glacier has been the target for many ongoing observations (Brown et al. 1982; Van der Veen 2002; Benn et al. 2007). Warren & Aniya (1999) describe calving glaciers of both tidewater and freshwater types in the South American Andes, with sites in Chile and Argentina. The significance of calving as an efficient form of mass loss has been documented for the Antarctic ice sheet (e.g. Jacobs et al. 1992) and Greenland's outlet glaciers (Higgins 1991; Box & Decker 2011; Benn et al. 2007).

2.2 Tsunamis

Generally, the term tsunami describes series of waves travelling on open water with a large wavelength (Shi & Smith 2003). The most devastating tsunamis are often triggered by oceanic earthquakes or subaquatic landslides and the waves travel with great speed in all directions (Berz et al. 2001). The dynamics of tsunami waves change as they approach the coast. Their speed decreases as they reach shallower water, increasing the height of the waves with the potential to flood long strips of coastline (Shi & Smith 2003). Waves reaching up to 30 m in height have been documented impacting the coast of Hawaii and Japan (Berz et al. 2001), sometimes travelling distances of 10,000 km. Large tsunamis pose significant hazards to low-lying coastal areas, causing destruction of infrastructure and the loss of life (Shi & Smith 2003). The tsunami risk has significantly increased over the past several decades due to the increased development of coastal areas from industrialisation and tourism (Berz et al. 2001).

2.2.1 Causes

The most prominent causes of severe tsunamis in recent history are subaquatic earthquakes or mass failures with the potential to trigger large scale waves with a high destructive potential (Berz et al. 2001; Garrett & Munk 2001). The tsunami that hit the coast of Papua New Guinea in 1998 was triggered by a submarine mass failure following an earthquake, causing massive damage in coastal zones and the loss of thousands of lives (Tappin et al. 2008). Only few years later one of the most devasting incidents in recent history was the tsunami following the 2004 Sumatra earthquake resulting in the loss of more than 200,000 lives across southeast Asia (Subarya et al. 2006). Yet, tsunami waves do not necessarily originate from earthquakes. Walder et al. (2003) describe various other causes in form of mass flow events as a potential source of tsunamis. Not only landslides but also debris avalanches, pyroclastic flows and rockfalls bear a high tsunami potential in the right setting, which are not limited to oceanic regions (Walder et al. 2003). Mass movement processes like this can both occur subaquatic and subaerial. This limits the tsunami potential not only to coastal areas around the world but also includes alpine regions with confined aquifers and steep slopes as potential tsunami regimes (Fritz et al. 2003). Besides high-density rock- and soil movements, Fritz et al. (2003) describe low-density processes such as snow avalanches and glacier ice fall as potential triggers of tsunami waves. In polar regions, these low-density mass movements have the potential to generate large waves, such that glaciers can be a major trigger of tsunamis (Long et al. 2015).

2.3 Dendrogeomorphology

The analysis of tree rings can be used as an accurate method of dating (dendrochronology) past physical events and processes (Stoffel & Bollschweiler 2009). This is possible in tree species which form distinct growth rings each year (Stoffel 2006). As geomorphology is the study of the processes changing the landscapes, both in the present and in the past, dendrogeomorphological approaches use the disturbances on living trees induced by physical processes to date past events (Lang et al. 1999; Stoffel & Bollschweiler 2009). The term dendrogeomorphology was introduced by Alestalo (1971) and refined

by Shroder Jr. (1978) noting that trees display various different growth responses to events caused by physical processes.

Shroder Jr. (1978) introduced the concept of 'process-event-response' whereby the physical processes of mass movement, such as landslides, rockfalls and floods which cause a mechanical disturbance to the tree growth, for example, the tilting of trees, burial of stem wood, scarring of the bark or rotting of wood material are identified. Trees react to these events through different growth responses, such as building reaction wood, suppression or termination of growth in extreme circumstances.

2.3.1 Dendrogeomorphology in shrubs

The analysis of shrubs in dendrochronology has found acceptance in a variety of fields, including dendrogeomorphology. In shrubs where annual growth rings are present, a multi-decadal record of changes in the surrounding environment can be discerned (Myers-Smith et al. 2015). This technique has been successfully used to reconstruct climate variations, ecosystem disturbances and in the reconstruction of geomorphological processes (Myers-Smith et al. 2015). Both annual growth responses and annual stem increments have been investigated with ring width measurements while disturbances have been studied by the examination of wood anatomy and wood scarring (Myers-Smith et al. 2015).

Prior to the start of the century, the application of shrubs in dendrogeomorphological techniques was not common (Gers et al. 2001). One of the first applications of this methodology was the reconstruction of landslides in Rheinhessen, Germany using *Crataegus oxyacantha* (Gers et al. 2001). By studying exposed tree roots, it is possible to reconstruct soil erosion rates (Gärtner et al. 2001; Gärtner 2007; Chartier et al. 2009) and this technique is also potentially applicable in the case of shrubs. The influence of rockglaciers and permafrost creep in high mountain environments on the growth of *Salix helvetica* has been studied on samples of both active and inactive rockglaciers (Roer et al. 2007; Gärtner-Roer et al. 2013). Although no significant differences in ring widths between stressed and unstressed shrubs, there appeared to be a difference in the size vessel lumen area, as stressed samples from active rockglaciers tend to have smaller vessels than unstressed (Gärtner-Roer et al. 2013). This shows the potential of a wood anatomical approaches in shrubs as a means to reconstruct physical processes (Gärtner-Roer et al. 2013).

In a pilot study by Buchwal et al. (2015) shrub growth was analysed and used to reconstruct a landslide-induced tsunami in West Greenland. Yet, due to the small sample size involved, a definitive conclusion regarding the applicability of such a technique in reconstructing this kind of event, is not possible.

2.4 Betula nana (dwarf birch)

During the fieldwork in July 2018 samples were taken from both *Betula nana* and *Salix glauca* (herein *Betula* and *Salix*, respectively). For capacity reasons only *Betula* samples were analysed while *Salix* was sampled for potential future analysis.

Betula nana (dwarf birch) is an Arctic shrub that is predominant in circumpolar regions and plays a major role in the greening of the Arctic (Hollesen et al. 2015). Dwarf birches are native to Arctic and

boreal regions and can be found in Greenland, Europe and western Asia (Eidesen et al. 2015) (Figure 5). It can also be found in more southern latitudes but only in mountainous regions like the Alps and the northern British isles and prefers moist, acidic and nutrient-poor sites (De Groot et al. 1997).

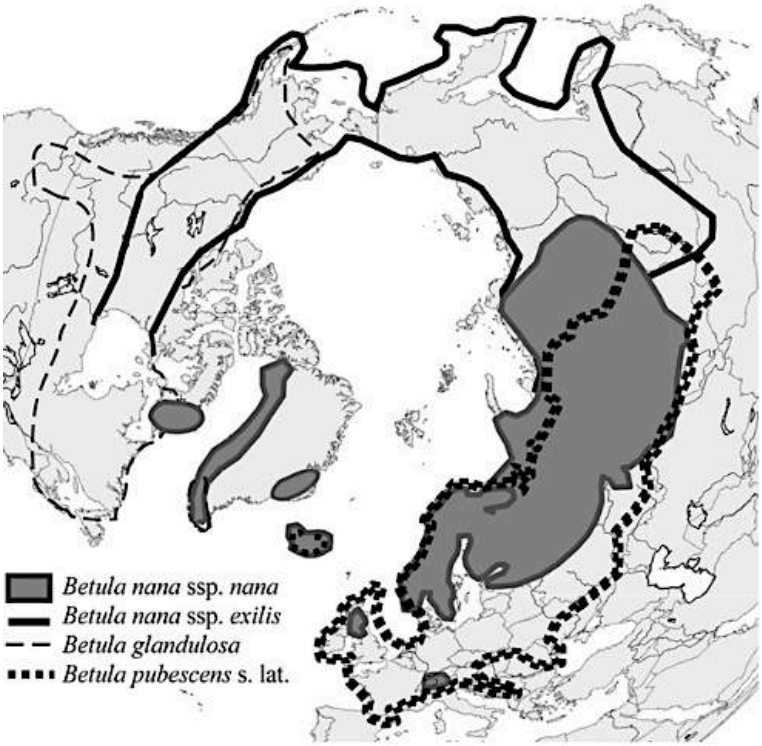

Figure 5: Circumpolar distribution of Betula nana (grey areas), as it can be found in West Greenland, Iceland, northern Eurasia and small parts in eastern Canada (Eidesen et al. 2015, p. 3995).

The young twigs of this strongly branching species are covered with resin spots and the small leaves (0.5-1 cm long) are dark green on the top (Hulten 1968) (Figure 6). The prostrate shrub growth on the ground up to a height of no more than 1 m, spreading its branches in a horizontal direction across the ground (De Groot et al. 1997).

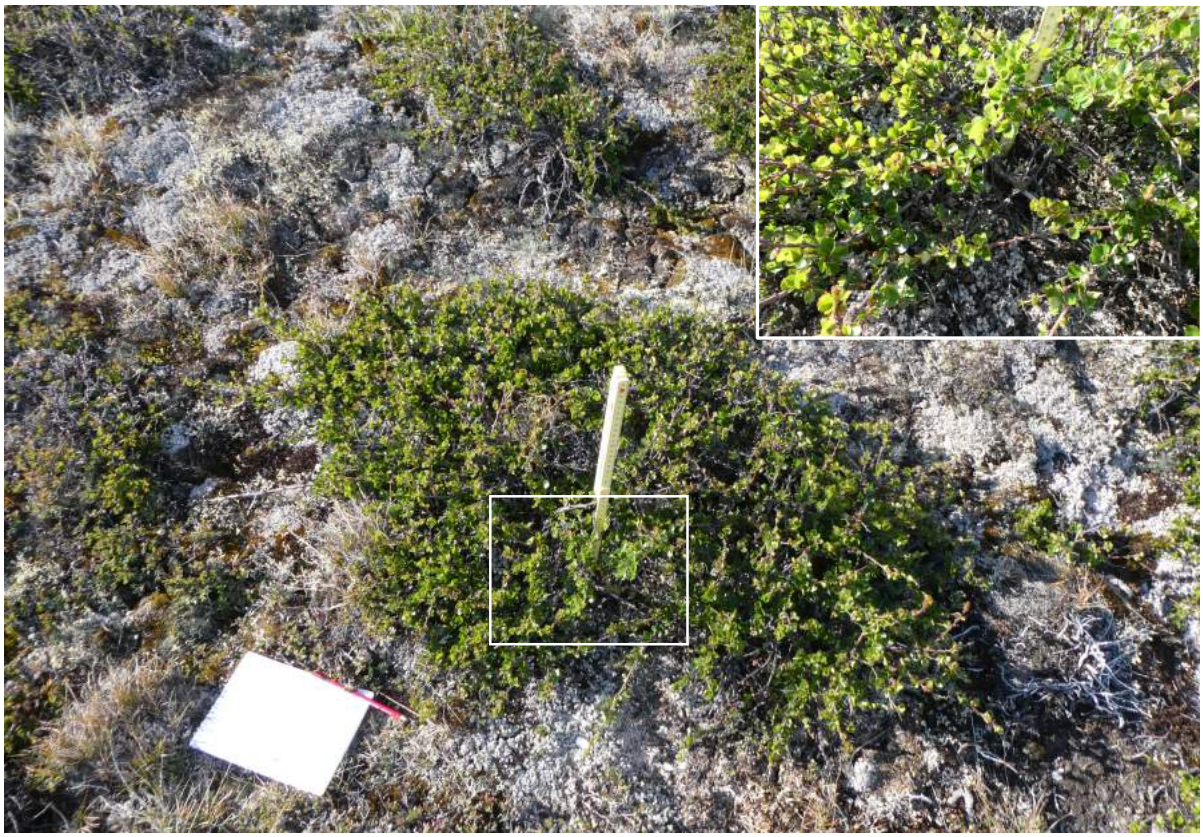

Figure 6: Betula nana shrub patch sampled in the reference zone during fieldwork in July 2018. The closeup shows the small lush-green leaves and juvenile twigs of Betula nana.

Betula species share common wood anatomical features such as labriform fibres and vessels (Schweingruber 1990). Amongst all *Betula* species *Betula nana* is the only species strictly classed as a shrub, whilst other members of the genus, under ideal climatic conditions, have a tree like form (Hellberg & Carcaillet 2003). Regarding vessel size, *Betula nana* can be distinguished from other *Betula* species by the smaller average vessel size and the larger number of grouped vessels (Hellberg & Carcaillet 2003). However, this makes the differentiation between small vessels and fibre cells more complex, as they do not differ significantly in cell size.

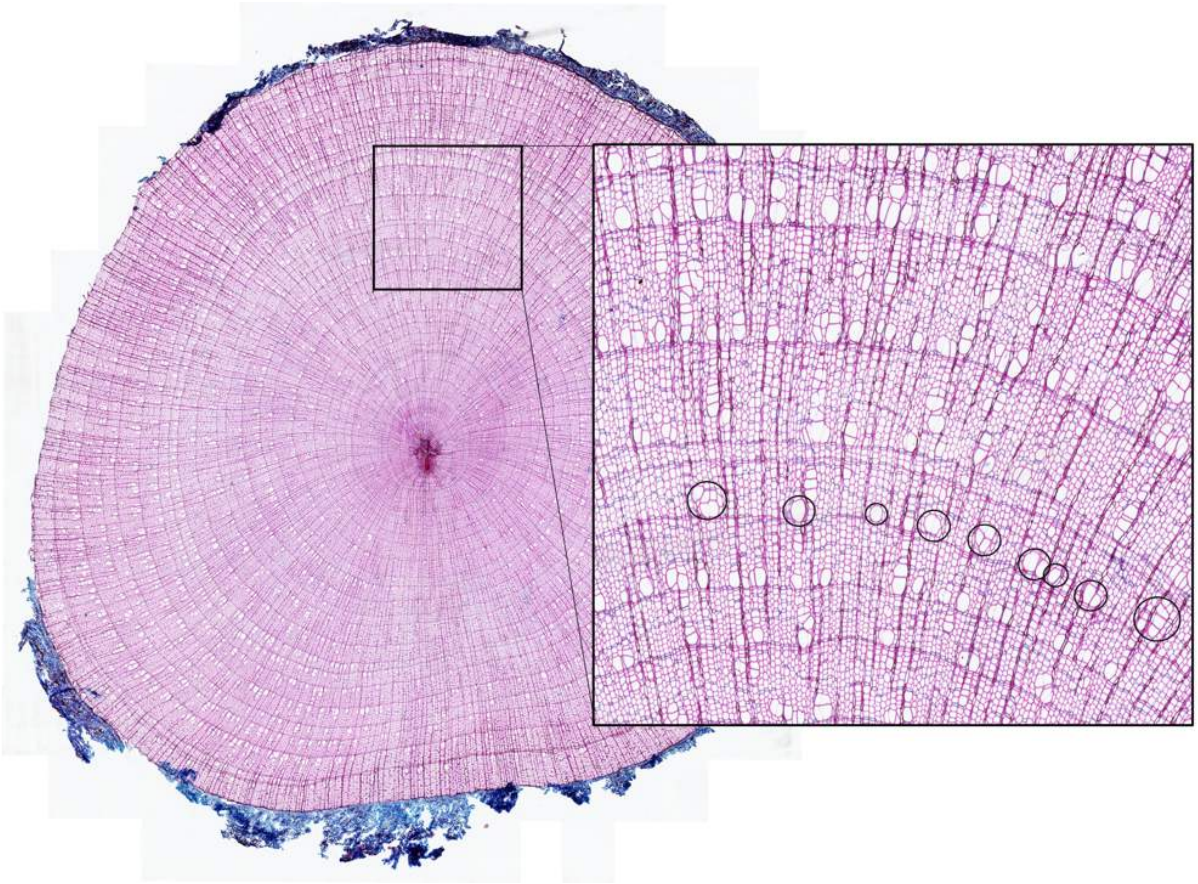

Figure 7: Cross section of Betula nana (B32_2r). The enhanced part displays large vessels (circled black for one year) and smaller fibre cells.

3 Study area

Greenland is the world's largest island, spreading over 24 degrees latitude with 2,600 km distance between southernmost and northernmost point (Machguth et al. 2016). The island is covered by one of the world's two largest ice sheets, which covers about 80 % of the island, while the remaining 20 % around the coast is ice free and habitable for Greenland's distinct fauna and flora (Cappelen 2018). The study has been conducted in West Greenland in the Disco Bay area (Figure 8). The Eqip Sermia outlet glacier is terminating into Kugsuak at the north-eastern shore of Disco Bay. Camp Eqi (69°45'N, 50°14'W), the base for our research, lies about 70 km north of the coastal town Ilulissat and is only reachable by boat. The camp includes the small glacier lodge consisting of a few huts run by 'World of Greenland', a tourism organisation with its local base in Ilulissat, and is only inhabited during the summer. Geologically, the area is dominated by a bedrock of granite and tonalite as well orthogneiss from granodioritic and tonalitic origin (www.maps.greenmin.gl). As the study area is in immediate proximity to both the sea and the Eqip Sermia glacier, in some areas the underlying bedrock is covered with fluvial and glaciofluvial deposits of undifferentiated origin (www.maps.greenmin.gl).

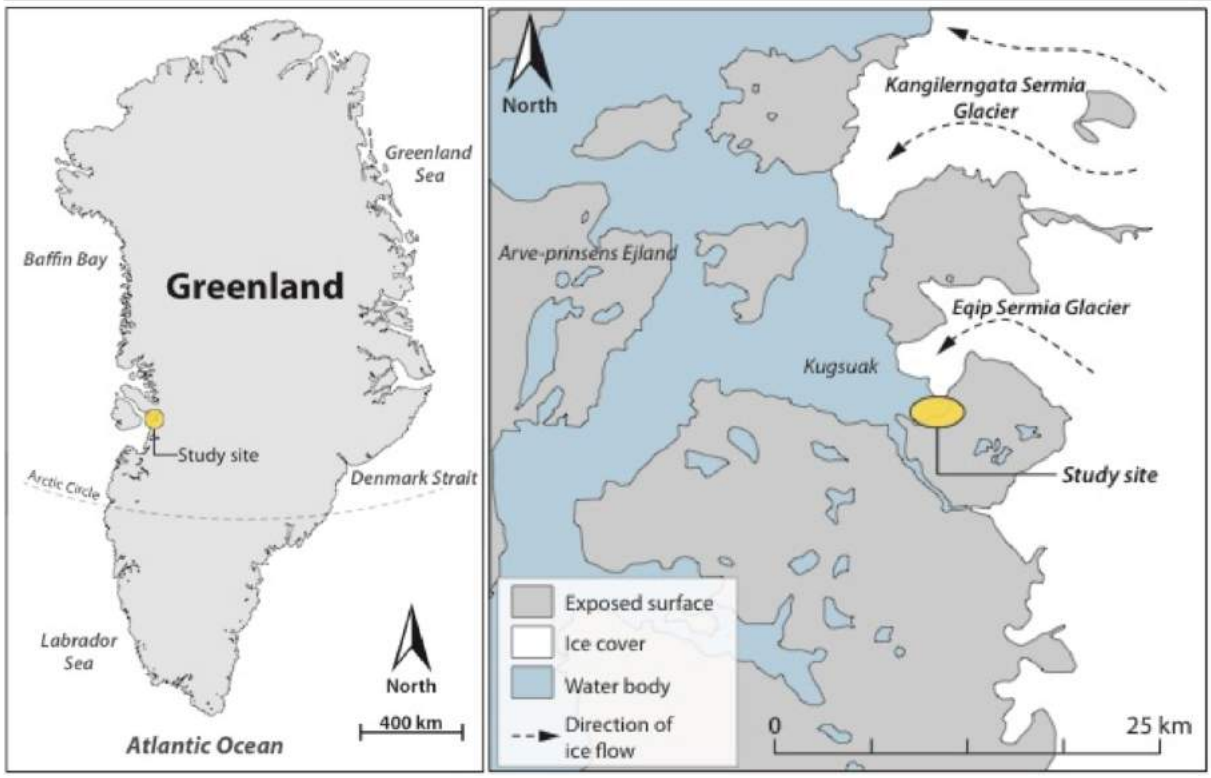

Figure 8: Location of the study site in West Greenland near Eqip Sermia glacier.

Greenland can be divided into different climate regions influenced by different varying conditions (Cappelen 2018) whilst the study site is located in north-western climate region. Ilulissat (69°13'N, 51°05'W) is the nearest settlement to the study area and is exposed to an Arctic maritime climate. The mean annual air temperature of Ilulissat is -3.9 °C, while the total annual precipitation for the town is 280 mm (Figure 9). Winter precipitation falls mostly in the form of snow, while in the summer season of June to August rain is more common, but with the chance of snowfall remaining (Cappelen 2018).

During the summer months the coastal areas of north-western Greenland frequently experience fog, since the weather is influenced by the sea (Cappelen 2018). As Ilulissat lies north of the Arctic circle it experiences the midnight sun/polar night lasting for 64 and 44 days respectively (www.timeanddate.com).

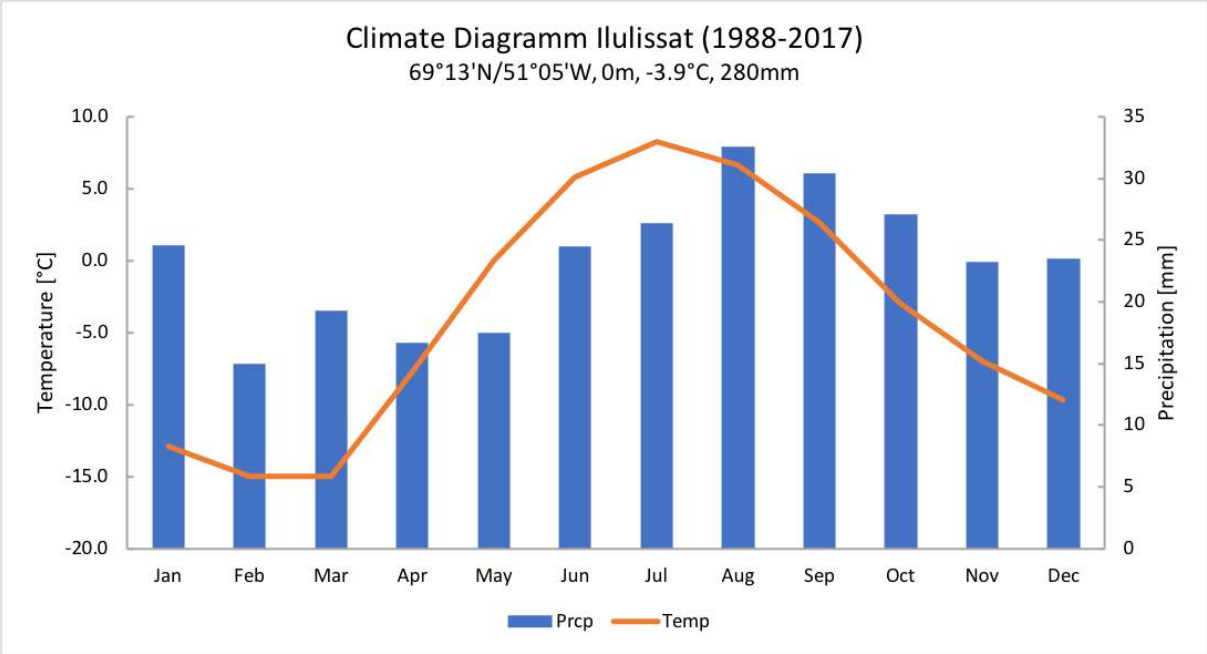

Figure 9: Climate diagram of Ilulissat with temperature data from the meteorological station in Ilulissat by the Danish Meteorological Institute (www.dmi.dk) *and precipitation data from a gridded KNMI dataset* (www.knmi.nl).

3.1 Study site Suicide Passage

The study site near Camp Eqi, where the shrubs samples were collected, is located at 69°45'44"N, 50°13'15"W, at a distance of 1.3 km from the camp. The area is called 'Suicide Passage', as there is a low-lying area between the fjord and a freshwater lagoon in the northwest, where the remains of the glacier moraine formed a natural crossing of the stream discharging the lagoon into the sea. This passage is frequently hit by glacier-induced tsunamis which can even transport small pieces of ice into the lagoon. The northeast directed slope of the study area is facing the Eqip Sermia glacier in a distance of 3-4 km to the glacier front. There is a strip low-lying beach in front of the field site, influenced by the tides of 10-30 m characterised by large boulders (>0.5 m). Above the beach, where waves have washed away the soil, smooth solid rock reaches up to the edge of erosion which was the border of the study area (Figure 10).

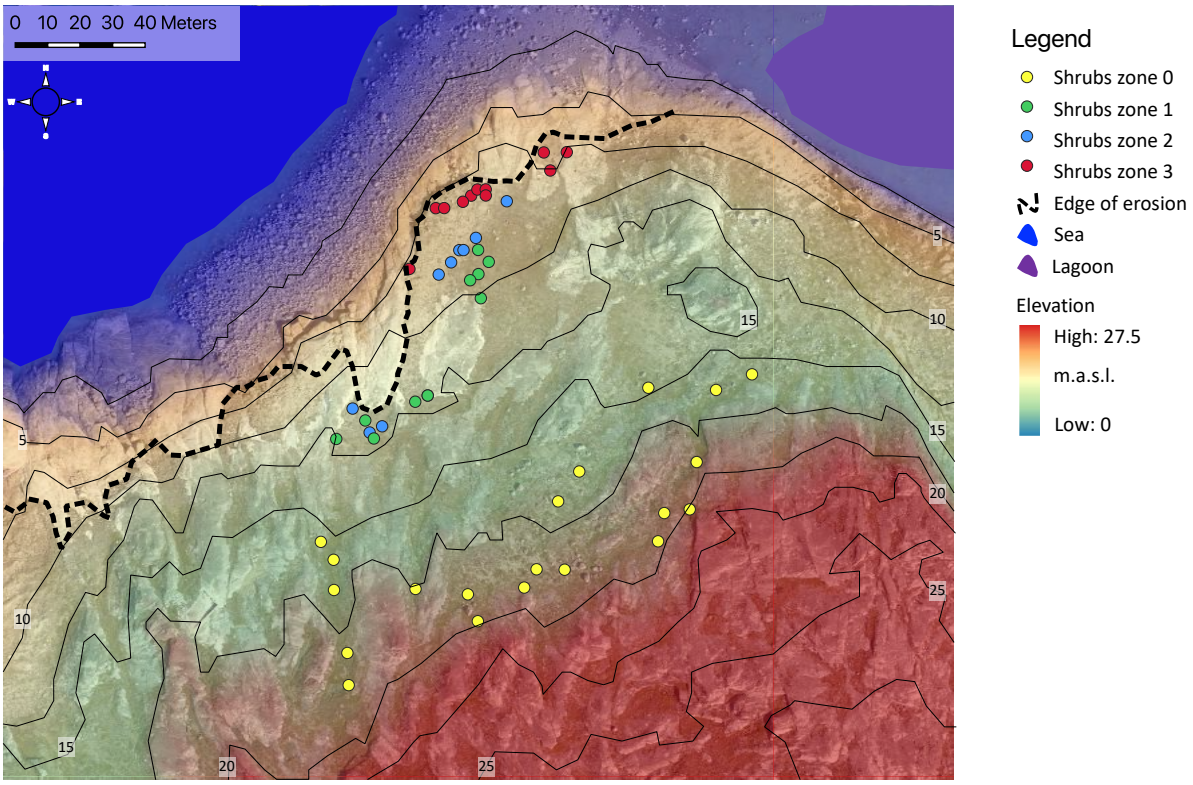

Figure 10: Positions of sampled shrubs in the study site (Suicide Passage) indicated with different colours of the specific sampling zone. Indicated with a dashed line is the edge of erosion and black lines indicate contour lines of the elevation in m a.s.l. (map data is based on aerial images taken during fieldwork in July 2018).

Above the edge of erosion, outside of the reach of tsunamis, the area is characterised by some large solid rock faces with vegetation growing in between on a thin layer of soil. Arctic shrub species like *Betula nana, Salix glauca* and *Salix arctica* can be found as individual plants or growing in larger shrub patches of 1-2 m^2 with sporadic occurrences of *Rhododendron groenlandicum*. Underlying and surrounding the shrubs, different mosses and lichen can be found which are also growing on the edges of the solid rock faces. Few flowering grasses and herbs make up a smaller part of the vegetation in the area.

3.1.1 Eqip Sermia glacier

The Eqip Sermia glacier has been the focus of multiple observations during the 20th century with the first observations dating back to 1912 by Alfred deQuervain (Lüthi et al. 2016). The area surrounding the Eqip Sermia glacier was the launching point for one of the first crossings of the Greenlandic ice sheet by deQuervain in 1912, chosen for the proximity and accessibility of the inland ice from the coast (Machguth et al. 2016). Since then multiple expeditions have been launched from the area, some of which also investigated the Eqip Sermia terminus glacier. The most significant expeditions are listed by Lüthi et al. (2016). Besides deQuervain 1912 also Wegener 1929-1931; the *Expéditions Polaires Françaises* between 1948 and 1953; the *Expéditions Glaciologiques Internationales au Groenland* from 1957-1960; as well as some further smaller observations have conducted studies of Eqip Sermia glacier. The frontal position of the glacier have been described since the first expedition and later campaigns

included that in their observations, by investigating changes of the glacier front since very early on (Zick 1972) (Figure 11).

The terminus position of the glacier has varied slightly during the past century but experienced a slow and steady retreat starting in 2000 in combination with an acceleration of flow velocity at the front (Lüthi & Vieli 2016).

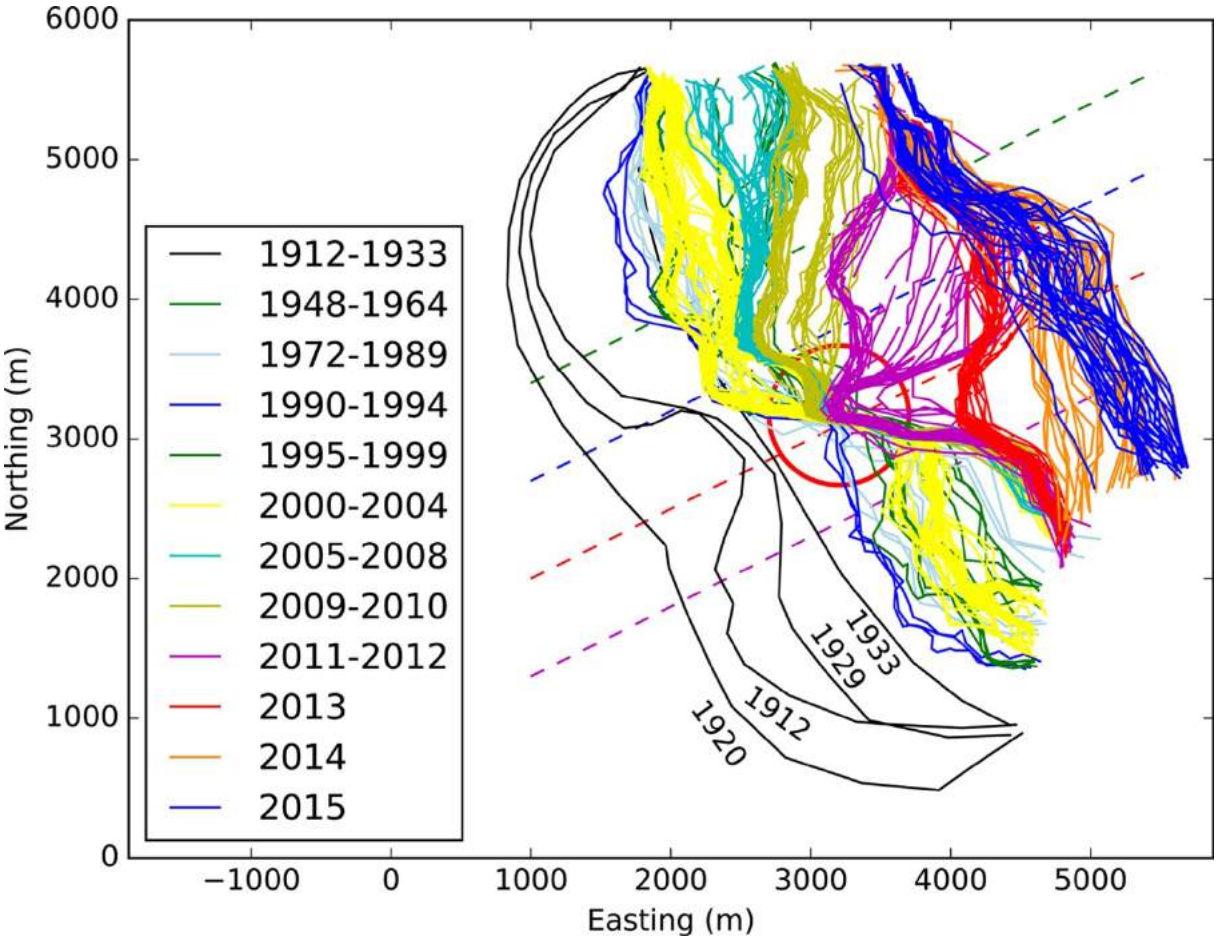

Figure 11: Historical front positions of the Eqip Sermia outlet glacier by Lüthi et al. (2016, p. 6)*. The red circle indicates the area in the central part of the glacier front where a steep ice cliff formed starting 2012.*

Lüthi et al. (2016) have analysed historic data of the frontal position extensively and combined them with recent observations of the glacier front, in order to estimate the retreat during the past century (Figure 11). After the first observations in 1912, the glacier advanced for a short period of time reaching its maximum of the 20th century in 1920. They observed the formation of two distinct lobes separated by the slow moving central part of the glacier front. Lüthi et al. (2016) explain the slow movement of the central part with the position of the bedrock beneath, which almost reaches the water surface, slowing down the flow of the ice. This shallow part of the fjord likely influences the individual retreat of the two lobes formed on both sides of the central part (Lüthi et al. 2016). Like the frontal position, the flow velocity was stable until 2000 with an acceleration up to 30 % between 2000 and 2005 (Rignot & Kanagaratnam 2006).

The most recent retreat of the glacier front starting 2010 was accompanied by a vast acceleration of the flow velocity reaching a speed of up to 12 m/d in 2014 (Lüthi et al. 2016). The two side lobes retreated individually with the right southern lobe being stable until 2013, and then retreating more than 1 km within only one year (Lüthi et al. 2016). Since 2015 the glacier front is more or less stable with a slow retreat as a result of the shallower bedrock topography beneath the current glacier front (Lüthi et al. 2016).

The special conditions of the bedrock topography favoured the formation of a steep and massive ice cliff of heights between 150-200 m in the northern part of the calving front (Lüthi & Vieli 2016). The bedrock height just below water level in the northern to central part of the calving front is likely the reason for the steep ice cliff observed after the latest retreats of 2012 and 2013 forming a maximum height of more than 200 m in 2014 (Lüthi et al. 2016) (Figure 12).

Figure 12: In the central part of the glacier front an ice cliff reached heights of 200 m. The red circle on the left marks dirty ice as an indication of proximity to the bedrock just beneath the water surface, the red circle in the centre marks a tour boat visiting the glacier front (Lüthi et al. 2016, p. 9).

The increase in the frontal height is expected to be the cause of the more recent phenomenon of large tsunami waves caused by collapsing ice at the calving front (Lüthi et al. 2016; Lüthi & Vieli 2016). Recent tsunamis have influenced and shaped the coastal vegetation and dynamics since the latest increase in glacier frontal height, causing soil erosion and death to the vegetation in close proximity of the waterline on the slopes facing the glacier (Lüthi et al. 2016). These observations could be confirmed during the field work conducted in July 2018. The erosion of the soil is evident in the study area and the influence on the vegetation close to the edge of erosion is highly visible (Figure 13).

Figure 13: View of zone 3 towards the edge of erosion with visible strong influences by glacier-induced tsunamis. Soil has been largely eroded and sand deposits around deceased vegetation indicates strong tsunami influence.

4 Material and Methods

4.1 Sampling design

The study area contains clearly identifiable evidence of tsunami occurrences and influences. The most distinctive characteristic is that of wave damage on vegetation. This is identifiable as deceased shrubs (close to the edge of erosion) or such in the process of recovering from damage (several meters further inland) (Figure 14). The affected area also shows geomorphological evidence, of soil erosion and deposition of marine sediments (sandy coastal sediments), found between both living and dead shrub patches which is also described in Buchwal et al. (2015). The presence of marine sediment deposits declines as distance from the edge of erosion increases. The deposition of relatively large rocks/boulders is indicative of a high energy tsunami, capable of transporting such material.

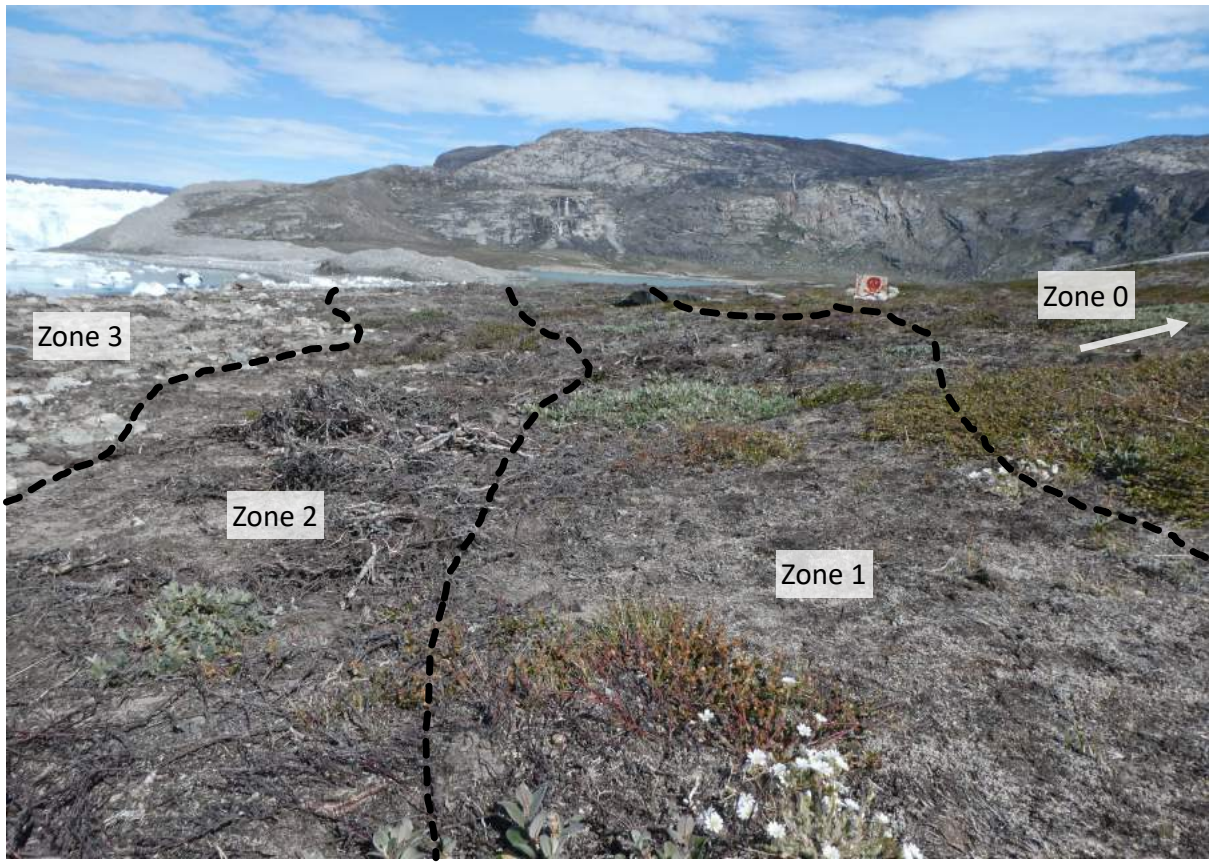

Figure 14: View of sampling zones of tsunami affected areas in the study site. In zone 3 strong tsunami influences are expected, in zone 2 intermediate influences and in zone 1 low influences. Zone 0 is located a little further up the slope and was used as a reference area.

As assumed *a priori* that the lack of vegetation in close proximity to the shoreline represents repeated tsunami inundation, preventing the establishment and recovery of shrubs. With increasing distance from the shore, such effects would be expected to decrease. As such, three different zones were identified: Zone 1 with assumed low tsunami influence (Z_1), Zone 2 with assumed intermediate tsunami influence (Z_2) and Zone 3 with assumed strong tsunami influence (Z_3). A control site (Z_0, no tsunami influence),

unaffected by tsunami influences, was selected 7-10 m above Z_1-Z_3 on the hillslope (Figure 14) but would still be subjected to the same microclimatic conditions as those experienced the affected sites.

Table 1: Overview over the zone characteristics of all sampling zones including the reference area.

	Zone 0	*Zone 1*	*Zone 2*	*Zone 3*
Number of samples	**20**	**10**	**10**	**10**
Impact	Reference zone	Low tsunami impact	Intermediate tsunami impact	Strong tsunami impact
Vegetation	Vegetation cover > 70%, Vegetation alive and in good condition	Alive or recovering > 50%, Living shrub patches, degree of vegetation higher	> 50% dead, Pioneer-plants present (lichen, mosses)	> 95% dead, No pioneer-plants, exposed roots
Soil	Soil intact	No erosion and intact organic layer, organic layer is dry	Soil intact with little erosion, Vegetation holds organic layer	Soil largely eroded, organic layer washed away
Deposition	No deposition	No visible deposition of marine sediments	No rocks > 10cm Sand deposition between plants, no driftwood	Boulders > 20cm Sand deposition > 50% Driftwood present
Additional features	Tsunami influence can be excluded based on topographic position	Dry surface as possible evidence of splash water from tsunami, Single events only	No signs of recent events, multiple events possible, Vegetation recovering from damage	Fresh evidence, repeated events likely, mechanical damage evident
Color	Greenish	Brown-green	Dark grey	Light grey
Avg Elevation [m.a.s.l.]	17.84	10.87	10.02	8.21
Exposition	NNE	N	N	N

In Z_0, 20 healthy looking specimens of both species *Betula* and *Salix* were chosen for sampling and a major branch of the shrub was selected to be cut and bagged for a wood sample. The reference plants were chosen based on an even distribution along the shoreline above the affected area in order to provide an even representation of the entire area (Myers-Smith et al. 2015).

For Z_1-Z_3 ten specimens from each species were selected for sampling. Unlike the reference area where only healthy-looking plants were selected, in Z_1-Z_3 affected shrubs, either dead or recovering, from tsunami influences were sampled. The immediate surroundings (1-2 m radius) of every sampled shrub needed to fulfil the above criteria of the specific zone of influence (Table 1). No shrubs were selected in areas where the transition between the different zones was not clearly visible. In the area showing signs of strong tsunami influence (Z_3) all sampled shrubs had died prior to undergoing sampling. Since there are vast amounts of driftwood and sand depositions present in this zone, only the shrubs that had intact roots in uneroded soil were selected.

From each zone, only large and mature shrubs were selected. If the shrubs grew in larger shrub patches, the main branch was selected. Shrub patches in some cases spread over 1-2 m^2 in which cases a large and accessible branch was singled out and sampled. For each shrub, we obtained wood material from both above and below ground. Depending on the specimen a larger piece could be sampled including the root collar or just above, in any case with enough material to enable the preparation of an above and below ground micro slice in the wood anatomy lab.

Figure 15: Sampling of a Salix glauca during the fieldwork in July 2018. A tape marked the position of the ground surface on the main branch, before the plant was carefully excavated and cut.

The selected branch was marked with a piece of tape at ground level and all the smaller branches around were removed before excavating the root (Figure 15). The upper side of the branch was marked with a black line on the tape to retrace its original positioning in the ground. The litter and soil below ground level was carefully removed to excavate the rooting part of the sample with at least 10 cm of below ground material. The sample was cut at least 10 cm above ground to retract the same amount of material above ground level.

After excavation, each sample was labelled with a unique six-digit code consisting of plant species (B = *Betula*, S = *Salix*), plant identification number (1-99), sampling zone (0-3) and the condition of the plant; alive (a), recovering (r), dead (d). For example, a living *Betula* sampled in the reference zone would be identified by the code: B01_0a.

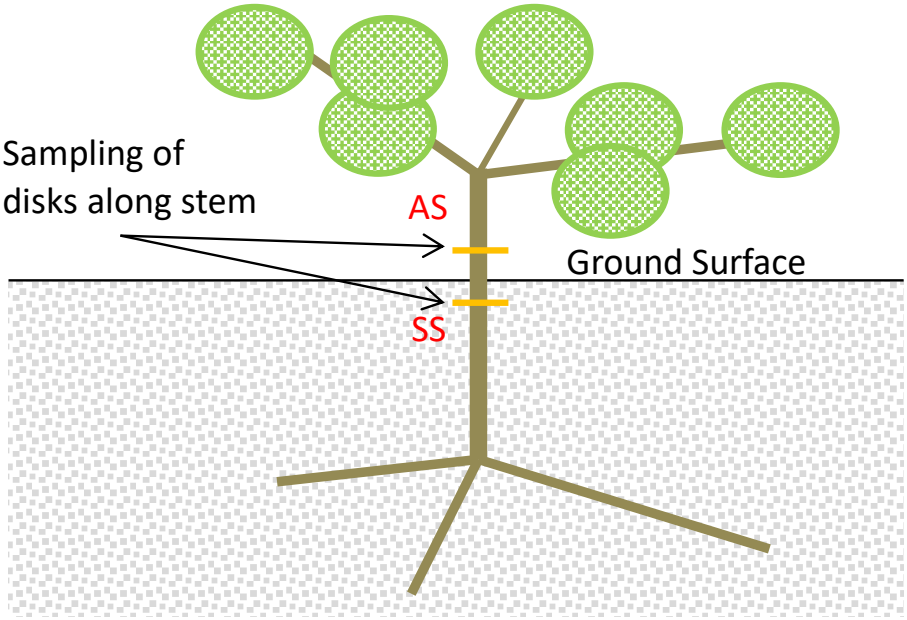

Figure 16: Schematic drawing of a sampled specimen indicating the positions along the stem, where discs were cut for further measurements. A tape was applied on the ground surface, enabling enough material for a below ground sample (SS) and an above ground sample (AS).

The information on the individual shrubs which were sampled can be found in the Appendix along with information on the individual sample age and average ring width (Table 13).

4.2 Sample preparation

The collected samples were returned to the 'Swiss Federal Institute for Forest, Snow and Landscape Research' (WSL) in Birmensdorf, in preparation for analysis. From each shrub sample a section of about 2 cm was excised just few millimetres above and below the tape to both capture above and below ground growth (Figure 16). In addition, every section was also marked with pencil to identify the samples later on. For capacity and workload reasons only *Betula* samples were processed and analysed. Samples of *Salix glauca* were archived for potential future analysis but not processed.

For each sample, micro sections for anatomical analysis were made, following the standard procedures (Gärtner & Schweingruber 2013 ; Gärtner et al. 2015). Samples were soaked in warm tap water for at least 30 minutes to soften the material prior to cutting. To distinguish the above and below ground sections, all micro sections received an additional code, (above surface (AS), sub surface (SS)). Using a WSL-Lab-Microtome (H. Gärtner et al. 2015), micro sections were cut from every shrub, from above and below ground. The small diameters of the shrubs samples (≈ 1.5 cm) allowed the cutting of entire cross sections of a thickness between 10-30 µm (Gärtner-Roer et al. 2013). A minimum of two replicas were made per sample in order to obtain a more stable quality of the resulting micro sections.

To produce a micro section, the sample was fixed in the holder of the microtome and cut with a disposable blade (Leica DB80). After obtaining an even surface following several pre-cuts, the

microsections were cut using an unused part of the blade and kept moist during the process. A thin paintbrush was used to transfer the sections to a microscope slide and a few drops of glycerol-water mixture (3:1 ratio) were added to prevent desiccation. The micro sections were then stored in a slide-storage map.

To stain and fix the micro sections on their microscope slides, a multistep-process was applied (Gärtner & Schweingruber 2013; Holger Gärtner et al. 2015; Gärtner-Roer et al. 2013). The applied glycerol was removed using water, before a Safranin-Astrablue solution (0.75 % Safranin and 0.75 % Astrablue mixed 1:1) was used to stain the thin section, for at least 3 minutes. Excess staining solution was rinsed from the sample with water before the sample was dehydrated using ethanol of increasing concentrations (75 %, 96 % and 100 %). Following the dehydration steps, the samples were rinsed in Xylol and imbedded in Canada-Balsam. Finally, all samples were oven-dried at 60 °C for 24-48 hours. Any dried Canada-Balsam residue on the cover glass was removed using blades to obtain a clean surface of the finished micro sections.

4.3 Ring Width (RW) measurement

4.3.1 RW measurement with WinDendro and WinCell

In order to measure the annual ring width of the samples, high resolution images were required to differentiate the individual rings of the shrubs. These images were obtained with a slide-scanner (model ZEISS Axio Scan.Z1 with a resolution of 0.441 microns per Pixel) at the centre for microscopy and image analysis at University of Zürich. The micro sections were cleaned with a sharp razor blade and placed into the scanner. The scanning of 100 slides took up to 48 hours and the resulting images were transferred to the WSL server for analysis. The raw files (.CZI) were then converted into .TIF format to analyse them in WinDendro and WinCell (www.regentinstruments.com) and the images were resized to 50 % to reduce the size of the individual files.

The ring width measurements from 2 radii of each microsection were carried out using WinDendro software. Each image was opened in the program and the longest radius was measured and set perpendicular to the ring boundaries. The rings were then measured from pith to bark starting with the innermost ring to the latewood boundary of the outermost complete ring. The samples were assumed to end with the year 2017 since they were cut in the beginning of July 2018, meaning that minimal earlywood had been formed, due to sampling taking place early in the growing season. A second radius was then measured in a different direction to verify the first measurement (Figure 17).

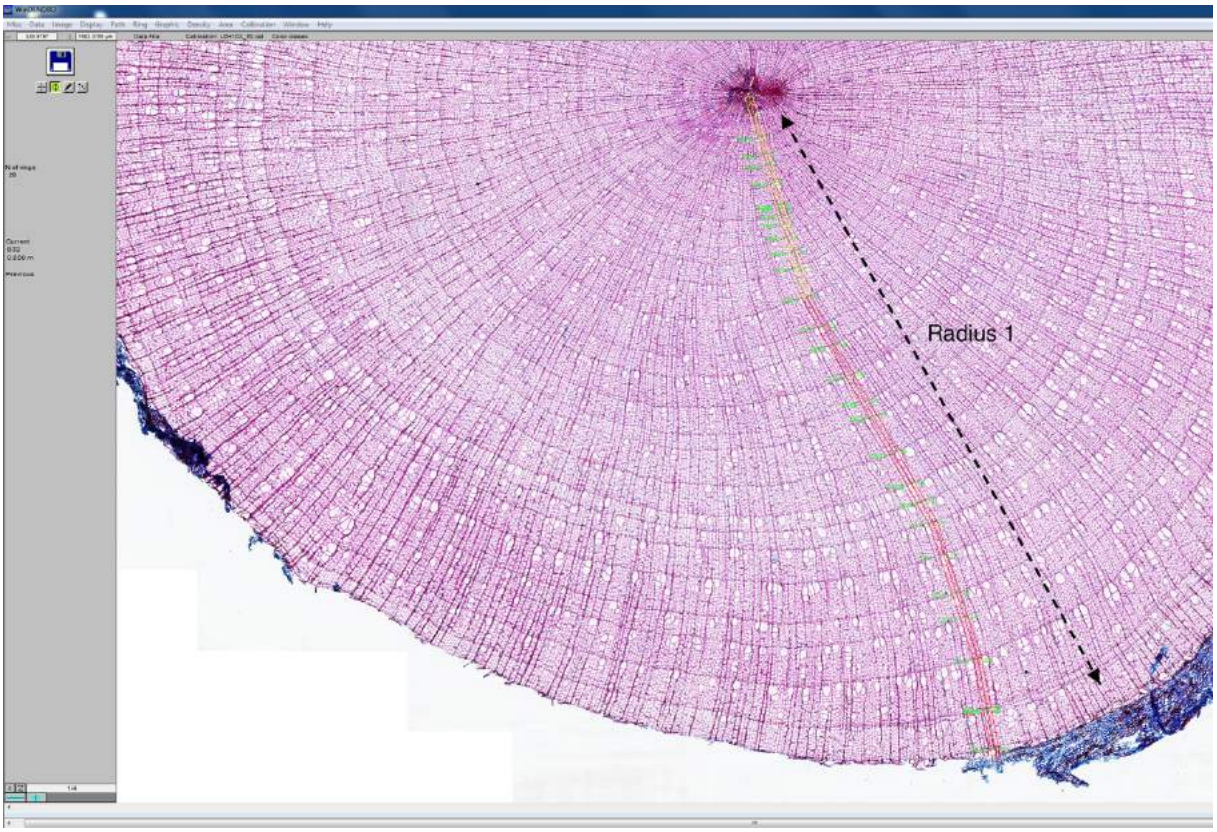

Figure 17: Ring width measurement in WinDendro on a cross section of B32_2r. On every cross section at least two radii were measured.

In cases where the files were too large for analysis in WinDendro (even after compression), the ring widths were measured using the path measurement tool of the WinCell software. Here, every ring width was measured with an individual path measurement along a predefined radius. Despite measurements being obtained in different software, the output is assumed to be the same, given the technique of measurement was not significantly different.

All the output measurements were converted into individual excel tables including the years for further analysis and crossdating.

4.3.2 Crossdating and building of reference chronology

In order to produce correctly dated rings series, crossdating (the comparison of patterns in ring width series) was conducted on all measurements (Myers-Smith et al. 2015). This was achieved through the visual and statistical comparison of the measured ring width series conducted in TSAP-Win (www.rinntech.de).

Due to the relatively young age of the samples (<70 years), crossdating was mostly conducted on comparison of the measurement series and not on statistical properties as described in (Buchwal et al. 2013; Rayback & Henry 2005). The growth series were visualized in the TSAP-Win software and the growth trends in the measurement curves were then compared in a hierarchical three-step process. In the first step the ring width series of the two radii measured in the same disk were compared to each other, secondly the average series of disks within one plant were crossdated and lastly the average series

of shrubs were compared within the entire population to detect all possible missing and partially missing rings. For the first two steps if a missing or partially ring (wedging ring) was detected, a NULL-ring was added to the measurement series. The third step was conducted in TSAP-Win software only and a value of 1 was assigned to added rings in order to detect them later on in the analysis process. Every added ring was carefully documented to make all the steps repeatable and retraceable.

To build the reference chronology the crossdated shrub averages from Zone 0 were first compared visually and the curves with the highest visual growth trend agreement were then again averaged to enable a comparison with other shrubs. One by one more plants could be fit into the chronology ending up with 13 plant averages to make up the final reference chronology (Buchwal et al. 2013). Gleichläufigkeit (GLK) describes the inter annual agreement of two chronologies comparing growth trends of both series and is expressed in a percentage of curve agreement (Kaennel & Schweingruber 1995). The GLK of every shrub average with the reference was then checked to ensure best possible fit for all the growth series.

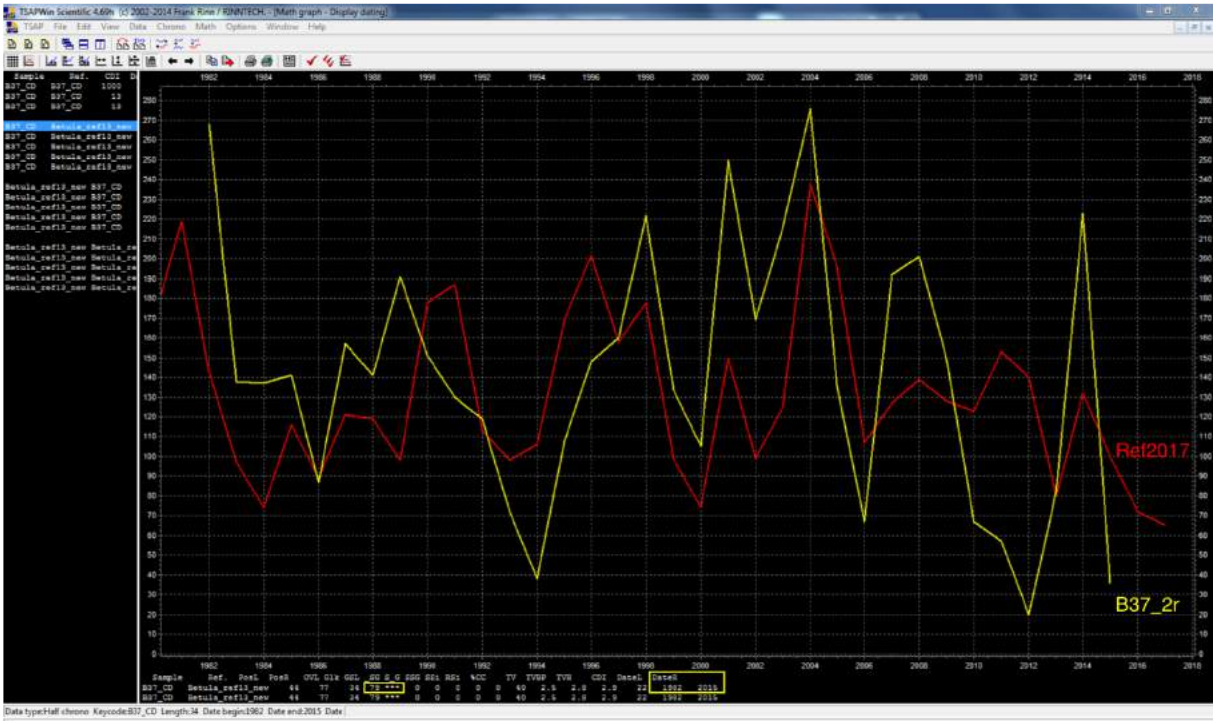

Figure 18: Crossdating in TSAP-Win by visually comparing B37_2r to Ref2017. The sample is dated to the year 2015 with a GLK of 79 %, reassuring the good visual match.

In a second step the shrub averages from Zones 1-3 (Z_1-Z_3) were compared to the reference chronology in order to precisely date each ring as in some instances the plants had died prior to sampling. The growth series from the shrubs were checked for a visual fit of the growth trend to the reference chronology (Figure 18). The highest possible GLK was used as a guidance meaning that the year-to-year agreement of the growth trend is as high as possible. An overlap period between the two curves of at least 20 years was required in order to properly date the sample. If necessary, a value of 1 was added if a missing ring was evident in a shrub, based on a ring being clearly present in the reference chronology.

The presence of a substantial number of missing and partially missing rings in the samples required careful and thorough crossdating in order to date all the samples correctly and to obtain a reliable reference chronology for the study area. Due to relatively short sample length, no age-related trends were expected and statistical detrending was not required.

4.4 Wood anatomical measurements

From all the obtained measurement variables by the program just the size of the vessels as vessel lumen area (VLA) in the shrubs was of interest. The measurements were conducted at the WSL image analysis Lab in Birmensdorf, using the WinCell software.

4.4.1 Global VLA measurements

For the global VLA measurements 7-10 samples from each zone (Z_1-Z_3) were selected for analysis. Selected samples needed to fulfil the following criteria: 1) both above ground (AS) and below ground (SS) cut in measurable image quality; 2) at least one sector of full radius in measurable image quality from pith to bark; 3) known age of shrub through crossdating. In Z_0 and Z_1 there were 10 shrubs each and in Z_2 and Z_3, 7 and 8 shrubs respectively that met all the criteria for the analysis.

From the original raw image files rectangular segments from pith to bark of one radius were cropped out in photoshop (version 5) for the measurements. The entire segment of every sample was then analysed as a whole using the WinCell software (Figure 19). The threshold for minimum and maximum vessel size was set for every analysed sample individually due to some differences between the shrubs. The threshold was set in a way that as many vessels were selected for measurement whilst excluding the maximum amount of the smaller fibre cells as possible. Still the distinction between vessels and fibre cells posed some difficulties, given the variability in the size of both cell types.

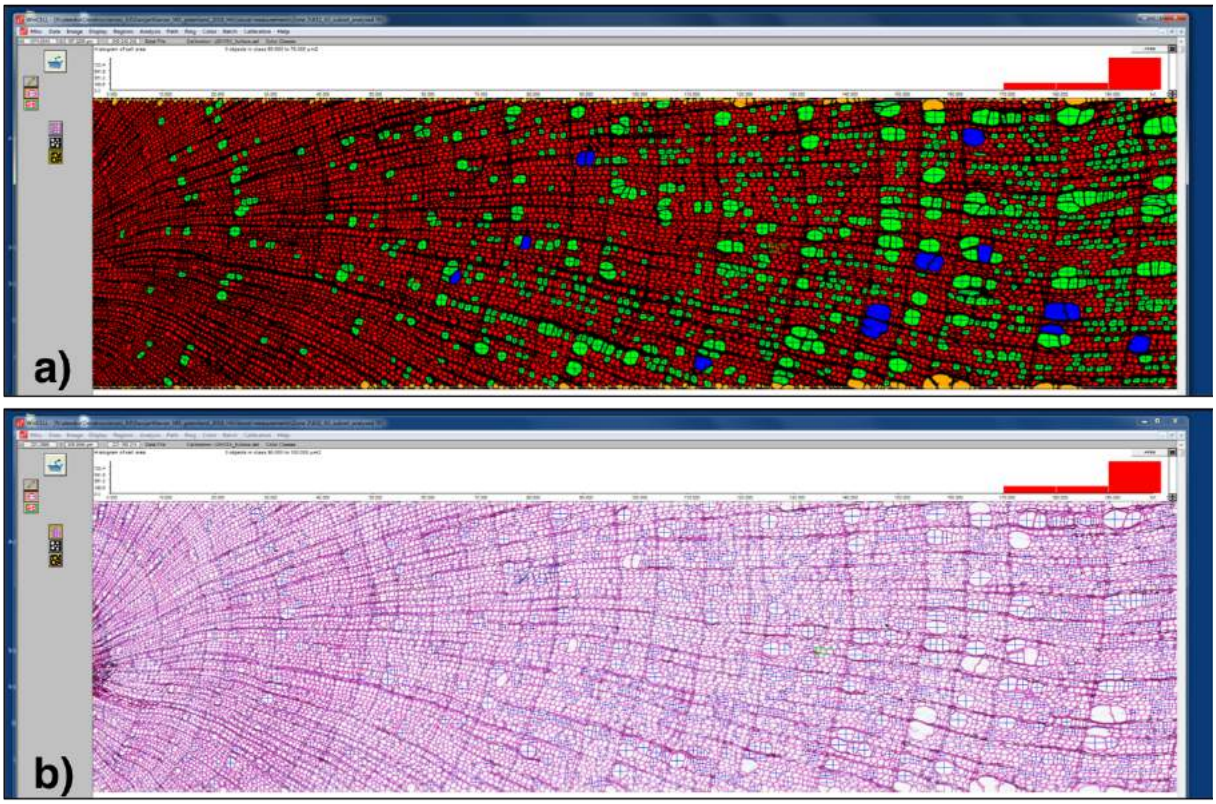

Figure 19: Global VLA measurement in WinCell on entire subset of cross section B32_2r_AS in a) false colour and b) real colour. In a) measured cells are coloured green, red indicated cell excluded by a filter and manually excluded vessel are coloured blue.

The outputs of the measurements were exported to Excel where the data was prepared for analysis by extracting only the year and VLA measurements. In addition to the VLA analyses, upper 25th percentile and the upper 10th percentile of measured vessels were extracted and analysed separately following a similar approach as used in (Gärtner-Roer et al. 2013). Determining the mean VLA of each shrub as well as means of above and below ground samples enabled not only a comparison of average VLA among the different zones but also differences in above and below ground vessels sizes.

4.4.2 Annual VLA measurements

As there are visible changes in vessel sizes within individual shrubs, annual VLA measurements of every zone were conducted to detect possible trends in vessel sizes. From each affected zone (1-3) seven samples were measured while from the reference zone a total of ten samples were analysed. They needed to fulfil the same criteria as for the global measurements and the ring boundaries needed to be clearly distinguishable. Measurements were only carried out on the above ground samples as the global VLA measurements did not show any significant differences between above and below ground vessel sizes (see chapter 5.4.2).

Using the WinCell software boundary tracing tool, ring regions were created for every year using the same rectangular segments as for the global VLA measurements (Figure 20a). In these ring regions the vessels were analysed for every year individually to detect tendencies over time in changes of VLA and number of vessels in each year. The threshold for these measurements was determined individually for

every analysed ring to measure just the vessels, excluding the fibre cells (Figure 20b). With individual thresholds it could be guaranteed that smaller vessels in the early growth years close to the pith were also detected and measured without excluding them by a globally set threshold.

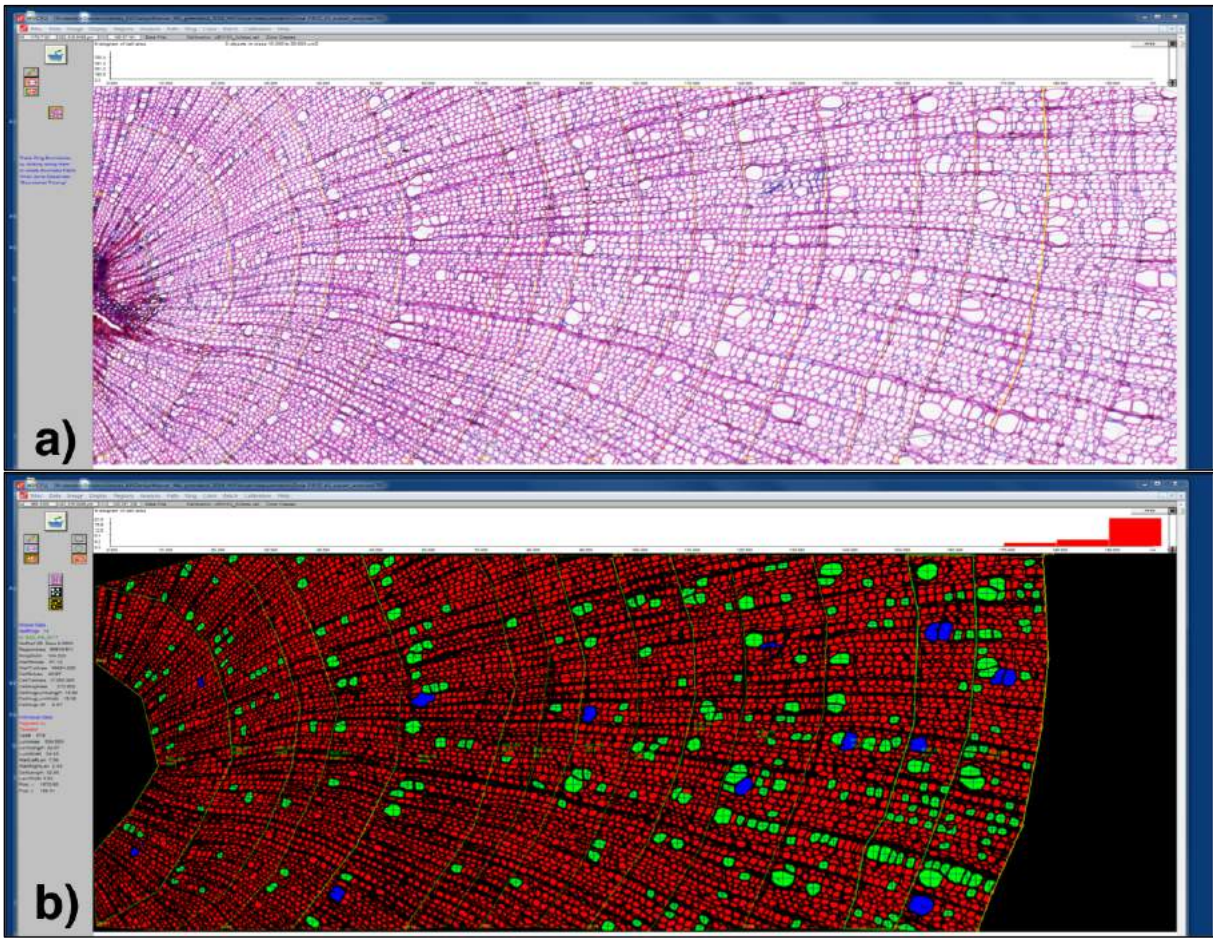

Figure 20: Annual VLA measurements in WinCell using the boundary tracing tool. Ring boundaries are traced manually in image a), in image b) VLA is measured in created ring regions (false colour image).

The measured cells were exported to and processed in Excel where the measured cells of every year could be differentiated. From the WinCell output of the ring regions also the ring width measurements of the analysed ring regions were extracted and crossdated as a direct comparison of the measured area. As they were measured only on the above ground samples and as an average of the ring regions, they might differ from the ring width measurements conducted in WinDendro before.

Some rings were too small, and no vessels could be detected. These years were included in the data table but left blank. The means, median for every year in every sample could be determined as well as minimum and maximum VLA as a guideline for the thresholds.

To process the data further, missing or wedging rings detected in the crossdating process needed to be added to get the specific and dated VLA measurements for each year. This step was crucial and even though the samples were crossdated with great care, a margin of error remains in this step.

4.5 Meteorological data

4.5.1 Soil temperatures

Soil temperatures were measured over a period of nearly 3 continuous years between 30.8.2014 and 24.10.2017. For the measurements 8 KB iButton temperature loggers of the type DS1922L (www.maximintegrated.com) with a resolution of ±0.0625 °C were used for these measurements, recording soil temperatures in an interval of 3 hours. The temperature loggers were deployed in peat soil near Camp Eqi (69°45'20.1"N, 50°15'09.2"W) in a distance of about 1.3 km from the study area at depths of (sensor 14gc1_1 = 16 cm, sensor 14gc1_2 = 9 cm, sensor 15gc1 = 16 cm and sensor 16gc1 = 12.5 cm). The sensors 14gc1_1 and 14gc1_2 were deployed at different depth during the same year and later replaced by just one sensor at the same location to continue the measurements. During the 3-year period, the loggers were retrieved twice to read out current records and replace them with fully charged ones. The records of the different loggers were combined to one single dataset for ground temperature, as there was no noticeable offset between loggers deployed in similar depth, the individual records are combinable to one continues ground temperature dataset.

Based on positive soil temperatures growing season (GS) was defined for July, August and September assuming to represent local conditions better than the traditional limit for the thermal growing season (Suni et al. 2003).

4.5.2 Temperature datasets

The nearest meteorological station to the study site with a continuous temperature record is located in Ilulissat and run by the Danish Meteorological Institute (DMI). A record of average daily temperatures exist for the time period from 1807-2017 with several gaps during the early years of measurement, the record however is complete from 1855 onward (Cappelen 2018). From this record, monthly averages of the air temperature as well as the annual mean temperature were calculated for Ilulissat.

As this climate station is located between 70 and 80 km from the study area, a gridded dataset of the exact location of the study site (69°13'N, 51°05'W) was derived from the KNMI Climate Explorer. Observational data of the CRU TS 4 atlas dataset was used to extract averages of the monthly near-surface temperature with a spatial resolution of 0.5° (www.knmi.nl).

4.5.3 Precipitation

Due to relatively low precipitation in western Greenland, it is more difficult to find continuous data. The DMI station in Ilulissat only has a continuous record of the accumulated monthly precipitation for a period between 1890-1984 (Cappelen 2018). As the analysed time period given by the reference RW chronology spans 1977-2017, precipitation data from the climate station in Ilulissat was of little use.

A gridded dataset could be extracted from the KNMI Climate Explorer from observational data of the CRU TS 4.01 atlas dataset (www.knmi.nl). The gridded dataset included the monthly averages of the daily precipitation for the time 1901-2017 as well as the annual mean daily precipitation. The monthly

averages were multiplied by the number of specific days in the respective month to receive a value for the total precipitation per month.
The hydrological year was quantified based on the end of growing season (1 October – 30 September) and total precipitation for growing season (GS) and non-growing season (NGS) were calculated, based on precipitation data from both current and previous year (Sargeant & Singer 2016).

4.6 Spatiotemporal mapping in QGIS

For the spatiotemporal mapping coordinates of every shrub and an aerial image of the study site were required. The location of each plant was recorded with a handheld GPS device (Garmin etrex VISTA Cx) with an accuracy of ±3 m. An aerial image was captured during the fieldwork with an eBee Classic drone (www.sensefly.com) recording with a spatial resolution of 4 cm per pixel. The drone covered a total area of 0.6km^2 and the high-resolution images were processed at University of Zürich. The processed image was georeferenced using the WGS84 reference system.
The shrub coordinates and the aerial image were loaded into QGIS (Version 3.4) (www.qgis.org) and visualised. The shrubs of Z_0 to Z_3 were symbolised using different colours (Z_0 = yellow, Z_1 = green, Z_2 = blue, Z_3 = red) in order to differentiate individuals of the different zones and analyse their distances to the edge of erosion.

4.7 Statistical analysis

The statistical analyses were conducted in Excel (Microsoft 2018) and the software package Minitab (version 18) and adopted a significance level of 95 %. Initially, the data sets were tested for normality using the Anderson-Darling test. For the comparisons of the means of two samples sets the two-sample Student's T-test was used. When comparing the means of all four zones an ANOVA was applied with the Tukey-Kramer post-hoc test to identify which groups were significantly similar.
To test for correlation of two individual datasets Pearson's correlation tests were applied in case of normal distributed data. If the data showed non-normal distribution Spearman's Rho was applied.

5 Results

5.1 RW measurements

5.1.1 Reference chronology

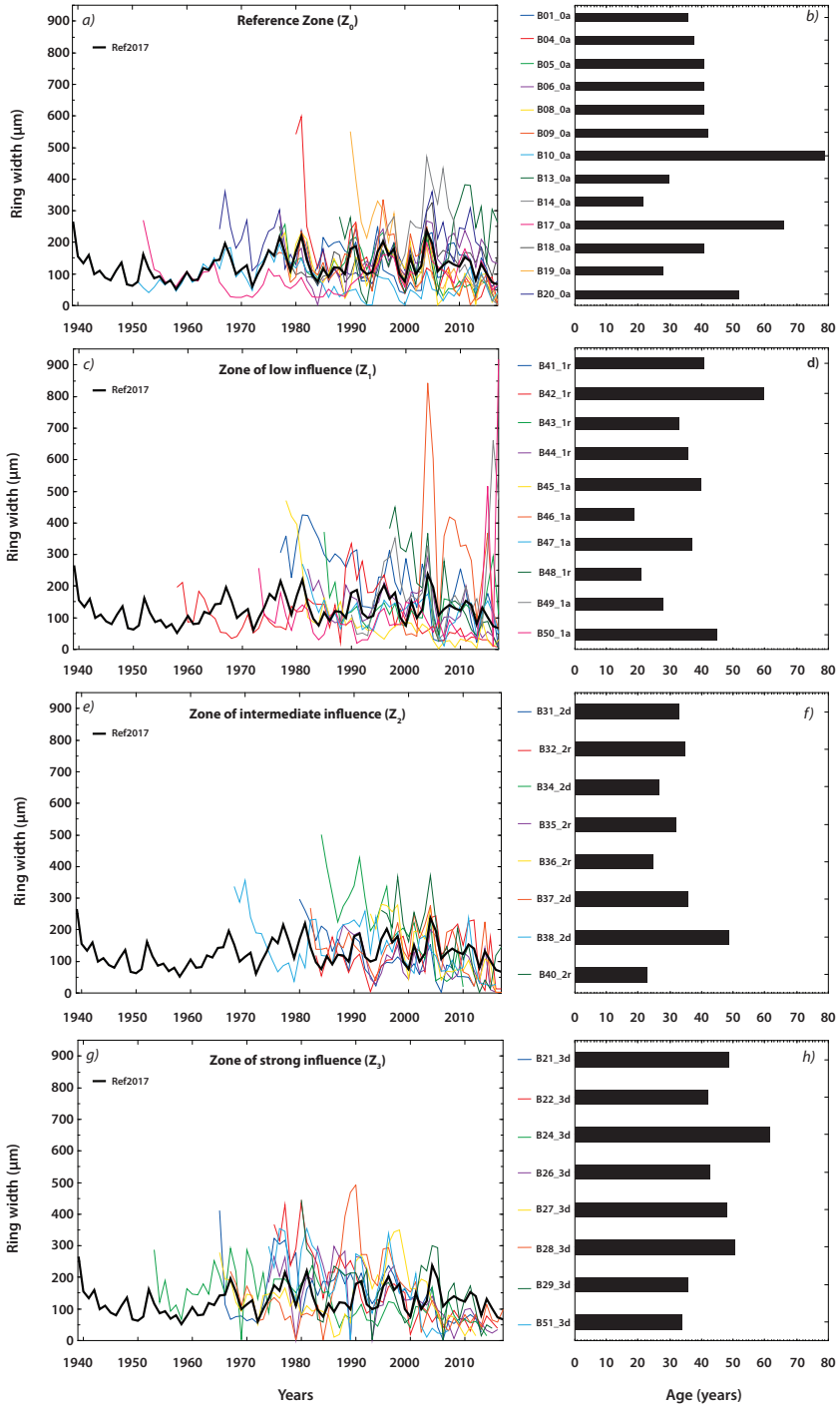

Figure 21: Crossdated growth series and individual sample age of all zones. a) Z_0, reference zone with no tsunami influence, n=13; b) age distribution Z_0, mean age = 43 years; c) Z_1, zone of low tsunami influence, n=10; d) age distribution Z_1, mean age = 36 years; e) Z_2, zone of intermediate tsunami influence, n=8; f) age distribution Z_2, mean age = 32.5 years; g) Z_3, zone of strong tsunami influence, n=8; h) age distribution Z_3, mean age = 46 years.

The reference chronology (Ref2017) is made up from a total of 13 crossdated shrubs collected in Z_0 (Figure 21a). The mean age of the plants in Z_0 is 43 years. The oldest sample (B10_0a) was 79 years old (three missing rings were added during crossdating), whilst the youngest specimen (B14_0a) is 22 years of age (no added rings) (Figure 21b). Prior to the year 1977, the chronology is created from four samples or less, whilst for the time period 1977-2017 more specimens were available. The average ring width for Z_0 shrubs is 139.58 µm (SD = 34.79 µm), with the highest and lowest average RW being 206.18 µm for B14_0a and 84.61 µm for B10_0a, respectively.

Table 2: The results of Pearson's correlation tests between individual chronologies of Z_0 and Ref2017, constructed by averaging these chronologies. Highlighted cells indicate a significant correlation (α=0.05).

	B01_0a	B04_0a	B05_0a	B06_0a	B08_0a	B09_0a	B10_0a	B13_0a	B14_0a	B17_0a	B18_0a	B19_0a	B20_0a
Correlation Coefficien	0.550	0.551	0.713	0.735	0.703	0.709	0.536	0.116	0.655	0.402	0.599	0.531	0.586
***p* -value**	0.001	<0.001	<0.001	<0.001	<0.001	<0.001	<0.001	0.542	0.001	0.001	<0.001	0.004	<0.001

With the exception of B13_0a, all specimens are significantly correlated with Ref2017 (Table 2). Despite B13_0a not showing a significant correlation with the reference chronology (p=0.5416), the visual agreement of the two curves is evident (Figure 21a) and was therefore not excluded from the reference.

5.1.2 Zone 1

The growth series in Z_1 show the highest average RW (156.47 µm) and variation (SD = 56.55 µm) of all zones (Figure 21c). The average age in Z_1 (36 years) is lower than in Z_0 with the oldest (B42_1r) and youngest (B48_1r) plant (being 60 and 21 years old, respectively) (Figure 21d). B48_1r is also the youngest sampled plant of Z_0 – Z_3.

Table 3: The results of Pearson's correlation tests between individual chronologies of Z_1 and Ref2017, (α=0.05).

	B41_1r	B42_1r	B43_1r	B44_1r	B45_1a	B46_1a	B47_1a	B48_1r	B49_1a	B50_1a
Correlation Coefficien	0.292	0.058	0.069	0.555	0.196	0.832	0.512	0.468	-0.128	-0.200
***p* -value**	0.064	0.662	0.701	<0.001	0.225	<0.001	0.001	0.032	0.516	0.187

The sample size in Z_1 is slightly bigger (n=10) than in Z_2 and Z_3 (n=8 from each zone). In Z_1, four plants are significantly correlated with Ref2017 (Table 3) with an average correlation coefficient of *0.592*.

5.1.3 Zone 2

The visual agreement of the individual growth series in Z_2 and the reference chronology is evident (Figure 21e). The individual plants show similar growth trends with respect to Ref2017. This is evidenced by the statistically significant correlation results shown in Table 4. The average RW (141.54 µm) is significantly similar to the RW of the reference zone (139.58 µm), (T_{14} = -0.12, p = 0.9066). The average age of plants in Z_2 is 32.5 years (±8 years) and as such considerably lower than the average age

of Z_0 (43 years). The oldest specimen (B38_2d) in Z_2 is 49 years while there are three plants (B34_2d, B36_2r and B40_2r) which range in age between 23 and 27 years (Figure 21f).

Table 4: The results of Pearson's correlation tests between individual chronologies of Z_2 and Ref2017, (α=0.05).

	B31_2d	B32_2r	B34_2d	B35_2r	B36_2r	B37_2r	B38_2d	B40_2r
Correlation Coefficien	0.272	0.491	-0.005	0.626	0.642	0.493	0.000	0.633
***p* -value**	0.126	0.003	0.979	<0.001	0.001	0.002	0.998	0.001

The statistical correlation of the specimens in Z_2 to Ref2017 is higher than those of the plants in Z_3; with an average correlation coefficient of *0.577* among the significant plants. Five out of eight plants show a significant correlation with Ref2017, whilst the remaining three plants show no statistical correlation but display visual agreement to the chronology Ref2017 (Table 4).

5.1.4 Zone 3

The average age of the individual shrubs in Z_3 (46 years) is 3 years older than the average shrub age in the reference zone. The coherency of RW chronologies in Z_3 is much less than that of Z_0, showing a higher SD of 18.13 µm (Figure 21g). The oldest plant is B24_3d dated at 62 years, with one added missing ring in crossdating (Figure 21h). The average RW in Z_3 is 150.44 µm which is wider than those in Z_0; though that is not statistically significant ($F_3 = 0.41$, $p = 0.7472$).

Table 5: The results of Pearson's correlation tests between individual chronologies of Z_3 and Ref2017, (α=0.05).

	B21_3d	B22_3d	B24_3d	B26_3d	B27_3d	B28_3d	B29_3d	B51_3d
Correlation Coefficien	0.264	0.343	0.217	0.295	0.299	0.208	0.547	0.372
***p* -value**	0.067	0.026	0.090	0.055	0.039	0.144	0.001	0.030

The statistical correlation of the individual Z_3-shrubs to Ref2017 is less evident than in the other zones, however, four out of eight plants (B22_3d, B27_3d, B29_3d and B51_3d) are significantly correlated with Ref2017 (Table 5). The average of significant correlation coefficients of Z_3 is *0.390*.

5.1.5 RW and tree age

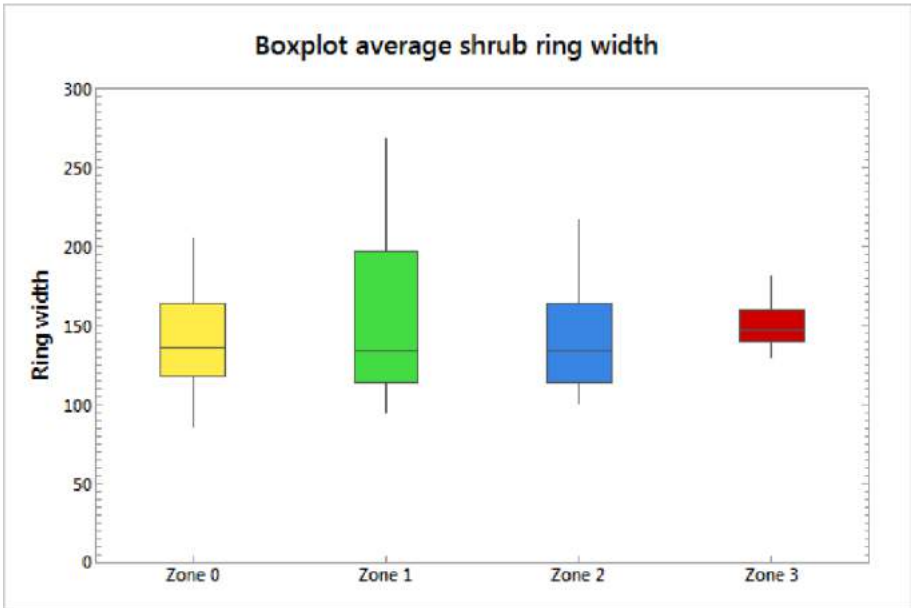

Figure 22: Boxplots of average RW comparing all zones.

There is no significant difference in average RW between the four zones (F_3 = 0.41, p = 0.7472) However, the observed variance of Z_3 (SD = 16.66 µm) is noticeably different to that of Z_0 and Z_2 (SD = 34.786 µm and 37.68 µm, respectively) and is less than half of the variance of Z_0 (Figure 22), while Z_1 is considerably higher than Z_0 and Z_2 (SD = 56.55 µm).

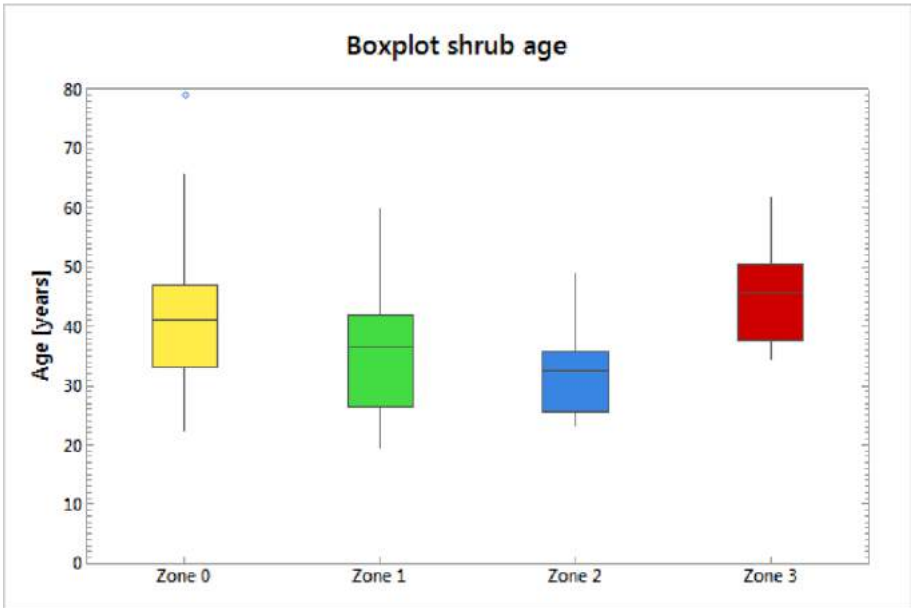

Figure 23: Boxplot of average shrub age comparing all zones. The blue diamond denotes an outlier value.

There was no statistical difference between the mean ages of sampled shrubs from each zone (F_3 = 2.18, p = 0.1083). However, there is a statistical difference between the average age of shrubs in Z_2 and shrubs in Z_3 (T_{13} = -3.06, p = 0.0091), with the plants in the latter being on average 13.5 years older than Z_2-shrubs. The variance of the plant ages from each zone shows that Z_2 and Z_3 are similar (8.18 and 8.96

years, respectively), whilst Z_0 and Z_1 display similar age variances (15.36 and 11.95 years, respectively) and are older compared to Z_2 and Z_3 (Figure 23).

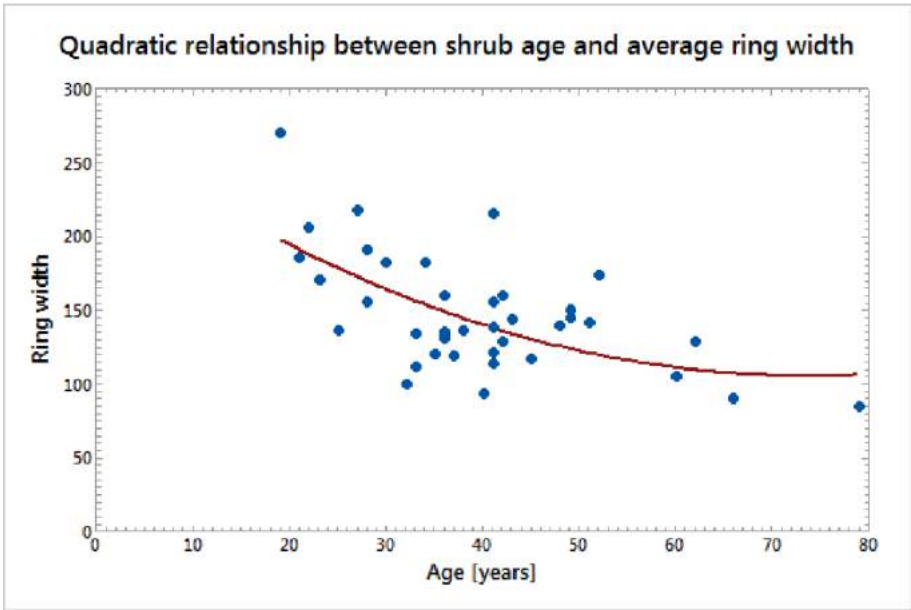

Figure 24: significant negative relationship between average RW and plant age.

A negative relationship exists between the mean RW and age of each sampled shrub; RW decreases with plant age ($F_2 = 10.46$, $p = 0.0003$) (Figure 24). The data was plotted in a quadratic regression (*R-sq*(adj) = 33.24 %) which is more suitable than a linear regression (*R-sq*(adj) = 31.23 %).

5.2 Callus tissue and reaction wood

The samples which underwent VLA measurements in WinCell were checked for visual disturbances such as reaction wood or callus tissue. Very few of these features were evident in the samples however, callus tissue was present in B40_2r (1982) as well as in shrub B46_1a (2004). Indications of reaction wood were detected in B40_2r (1979), B35_2r (1991) and B36_2r (1996) (Table 6). Other samples showed no visual sign of mechanical disturbance in the analysed sections.

Table 6: Years of containing callus tissue and reaction wood.

Year	Description	SampleID
1979	Reaction wood	B40_2r
1982	Callus tissue	B40_2r
1991	Reaction wood	B35_2r
1996	Reaction wood	B36_2r
2004	Callus tissue	B46_1a

5.3 Reconstruction of event years

5.3.1 Visual determination of disturbances

The crossdated growth series of every single shrub was compared to the reference chronology (Ref2017). In particular, the years of decreased relative growth affected multiple shrubs of the same zone in a specific year. Disturbances in individual shrubs were of interest when negative growth reactions compared with Ref2017 were detected in multiple specimens in the same year. For example, B51_3d shows clear negative growth reactions in the years 1997 and 2002 (Figure 25).

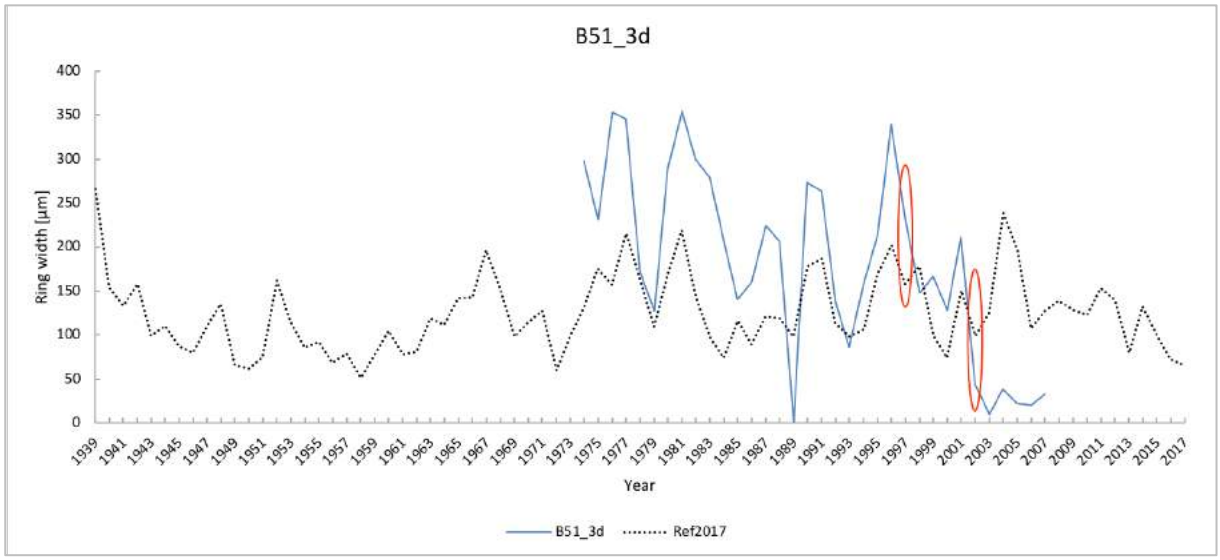

Figure 25: B51_3d shows negative growth reactions in 1997 and 2002 while the growth series correlates with Ref2017 (p=0.0303).

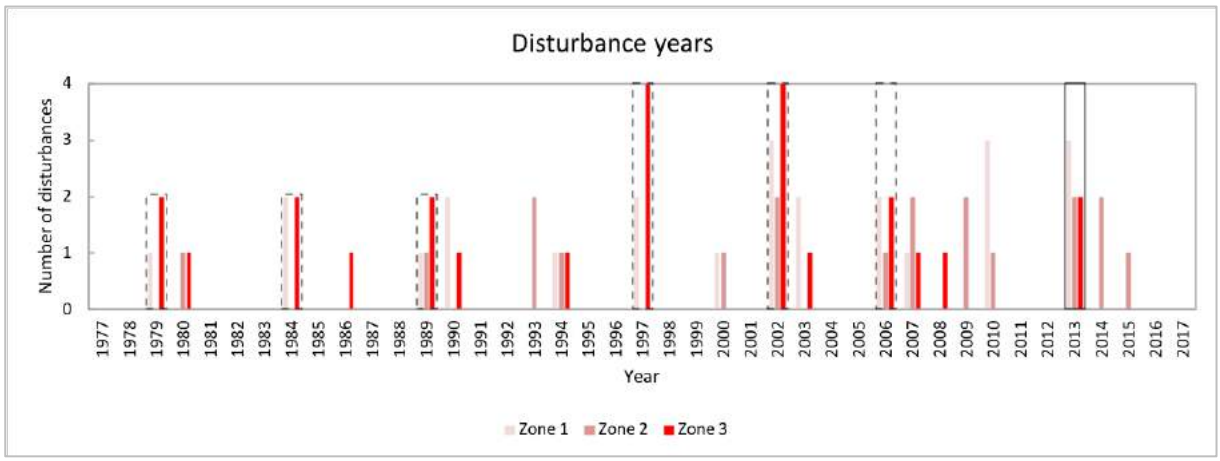

Figure 26: Disturbance years of growth series vs. Ref2017 with highlighted years 1978, 1984, 1989, 1997, 2002, 2006 and 2013.

Disturbance years were identified for four years 1979, 1984, 1989, 1997, 2002, 2006 and 2013, in 3 to 9 shrubs, occurring throughout Z_1-Z_3 (Figure 26). In these years at least two shrubs in Z_3 showed a decrease in growth compared to Ref2017. In 1997 and 2002 the effect is most evident with disturbances noted in 4 out of 8 plants in Z_3 (Table 7).

Table 7: Disturbed shrubs in Z_1-Z_3 for the years 1979, 1984, 1989, 1997, 2002, 2006 and 2013.

	Zone 3	Zone 2	Zone 1
1979	B21_3d, B27_3d		B42_1r
1984	B26_3d, B51_3d		B41_1r, B44_1r
1989	B21_3d, B22_3d	B37_2r	B44_1r
1997	B24_3d, B28_3d, B29_3d, B51_3d		B41_1r, B42_1r
2002	B22_3d, B24_3d, B29_3d, B51_3d	B32_2d, B34_2d	B42_1r, B48_1r, B50_1a
2006	B26_3d, B28_3d	B35_2r	B47_1a, B50_1a
2013	B24_3d, B26_3d	B32_2d, B38_2d	B43_1r, B44_1r, B49_1a

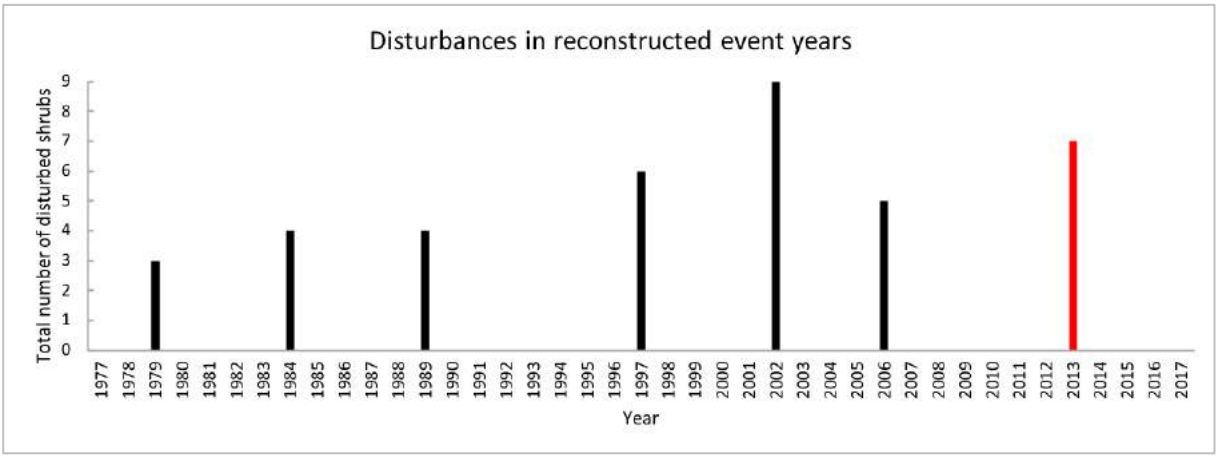

Figure 27: Total number of disturbed shrubs during years with assumed tsunami activity. The red bar indicates the tsunami event of 2013 described in (Lüthi & Vieli 2016).

5.3.2 VLA individual plants vs. VLAref

Similar to the assignment of disturbances in plant growth (as determined by RW), measurements of the annual vessel lumen area (VLA) of each individual shrub was compared to the VLA reference of Z_0. The VLA reference of Z_0 consists of 10 measurements (n=10), while in Z_1 – Z_3 7 plants from each zone were analysed (n=7).

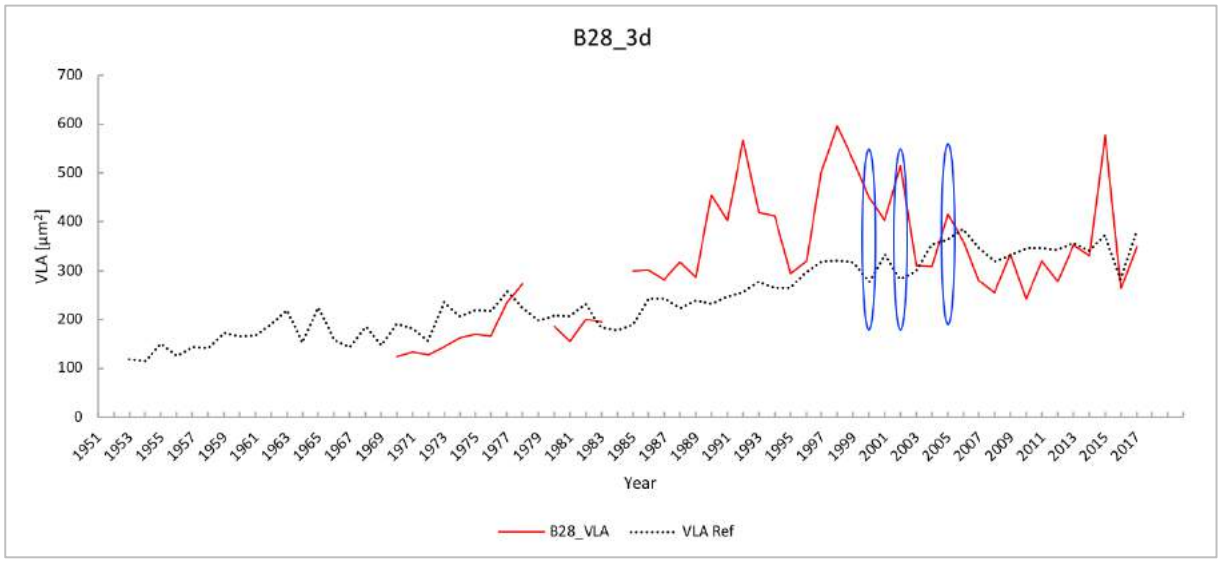

Figure 28: B28_3d shows asynchronous growth in VLA compared to VLA Ref in 2000, 2002 and 2005.

For example, B28_3d shows asynchronous changes in the VLA in the years 2000, 2002 and 2005 (Figure 28). In these years, the vessel size increases in VLA Ref while a visible decrease occurs in the VLA curve of shrub B28_3d. The disturbances noted in the single plants were collected and plotted per zone.

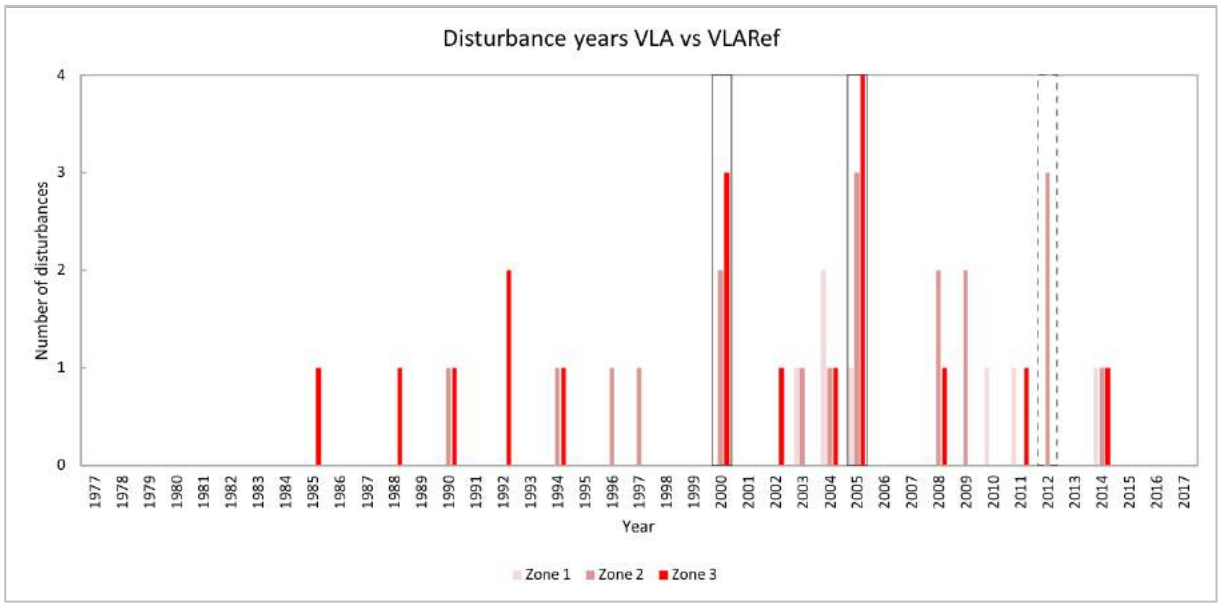

Figure 29: Disturbance years of VLA vs. VLAref with highlighted event years 2000 and 2005 as well as potential event year 2012 (dashed line).

Figure 29 shows that the years 2000 and 2005 contained notably more disturbances (a total of 5 and 8 disturbances respectively). In Z_3 for example, 4 out of 7 shrubs indicated a decrease in VLA compared to the reference Z_0 in 2005. The year 2012 yields 3 affected plants in Z_2. The remaining years (1985–2014) show no disturbances that considerably stand out.

Table 8: Disturbed shrubs in Z_1-Z_3 for the years 2000, 2005 and 2012.

	Zone 3	Zone 2	Zone 1
2000	B22_3d, B24_3d, B28_3d	B37_2r, B38_2d	
2005	B21_3d, B26_3d, B28_3d, B29_3d	B35_2r, B36_2r, B38_2d	B41_1r
2012		B35_2r, B36_2r, B40_2r	

In the year 2000, a total of 5 shrubs displayed an affected vessel size, distributed within Z_3 and Z_2 (Table 8). In 2005, a total of 8 affected plants can be found in all three zones. Seven out of these 8 are found in Z_2 and Z_3 while only one can be found in Z_1. The effects of changes in VLA occurred in a total of three plants in the year 2012 all of which were found in Z_2.

5.3.3 Mortality years

A total of 11 plants had died prior to sampling during July 2018 and their ages were determined through crossdating of RW with Ref2017. For these shrubs, the last measured ring would indicate their time of death. Plant B51_3d died in 2007 and B34_2d died in 2010. From year 2012 until 2017, a total of 9 plants died, at a frequency of at least one plant per year. In 2012, two shrubs (B27_3d and B31_2d) and in 2016 three shrubs died (B22_3d, B26_3d and B38_3d) (Figure 30). Approximately 73 % of deceased sampled plants grew in Z_3 close to the edge of erosion, while the remaining deceased plants were located in Z_2.

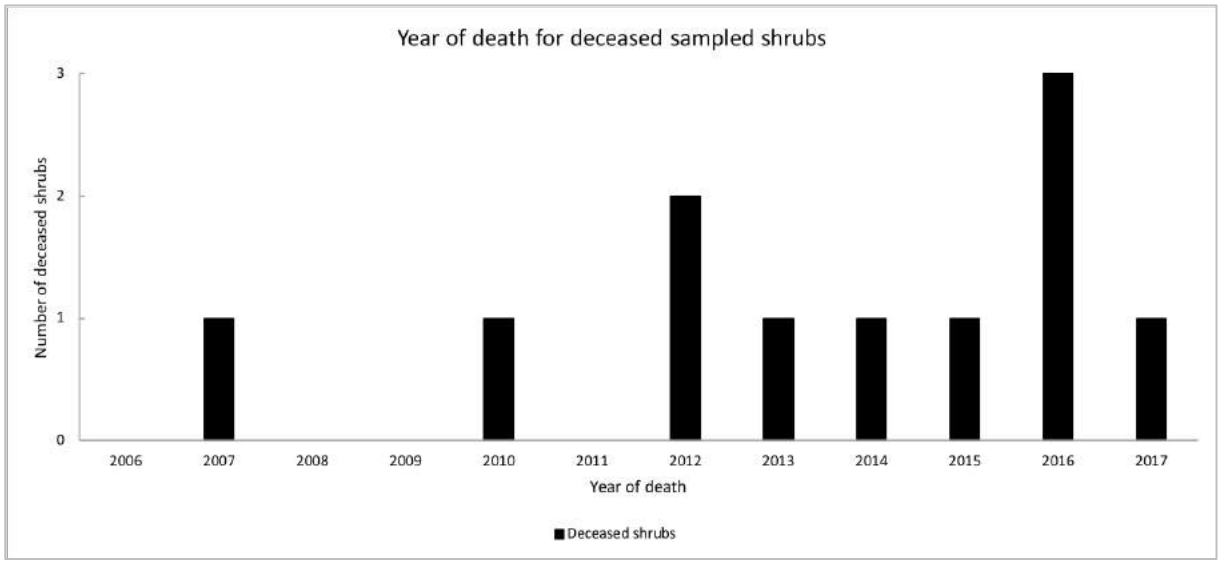

Figure 30: Year of death for all deceased shrubs sampled.

5.4 VLA measurements

5.4.1 VLA Z_1-Z_3 annual average and VLAref

The annual VLA measurements were averaged for each zone to compare them to the VLA reference from Z_0. First the VLAref was tested for correlation with the general ring width growth (Ref2017) and there is no significant correlation between annual VLA and the chronology ($r_s = 0.002889$, $p = 0.9857$). The average VLA in Z_2 and Z_1 is 29 % respectively 8 % smaller than the average VLA of the reference,

whilst Z_3 indicates 17 % larger VLA than the reference for the period between 1983 and 2005 before it drops under the average VLA of Z_0. In general, the average VLA in Z_1 are closer to the reference curve than the average series of Z_2 (Figure 31).

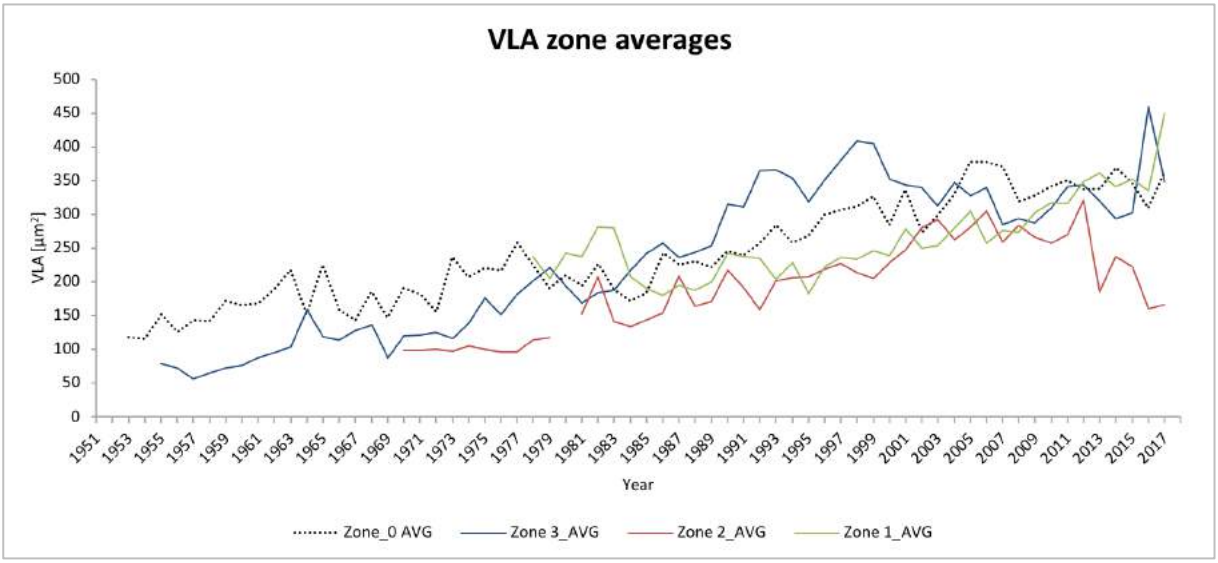

Figure 31: Average annual VLA Z_1-Z_3 compared with VLA_{Ref} of Z_0.

The VLA series of each zone (Z_1–Z_3) was compared to that of Z_0 in order to detect decreases in VLA in specific years. The years where a zone showed decreasing VLA averages while the reference increases, are shown in Table 10.

Table 9: Years with zonal VLA decrease compared to VLARef.

Year	**Z_1**	**Z_2**	**Z_3**
1984			
1991			
1994			
2002			
2003			
2004			
2008			
2010			
2016			

Z_3 indicates decreasing vessel sizes in five years (1994, 2002, 2004 2010 and 2016) although the average VLA for 2016 is based on an average of less than 5 specimens. Z_2 also shows signals in recent years (1991, 2003, 2008 and 2010) while Z_1 does not show any clear signals after 1994 and does not seem to have been recently affected. The year 2010 stands out in terms of zonal VLA decreases in both Z_2 and Z_3 compared to the reference.

5.4.2 VLA above ground (AS) vs below ground (SS)

The global VLA measurements were conducted on the entire sections of each sample, not differentiating individual years for the vessel measurements. The thresholds were set for the entire section and all vessels were analysed. The analysis was conducted on all measured vessels (Figure 32a), the upper 25th percentile and upper 10th percentile (Figure 32b & c). Global measurements were conducted on both above (AS) and below ground (SS) sections [n_{Z0}=10, n_{Z1}=10, n_{Z2}=7, n_{Z3}=8].

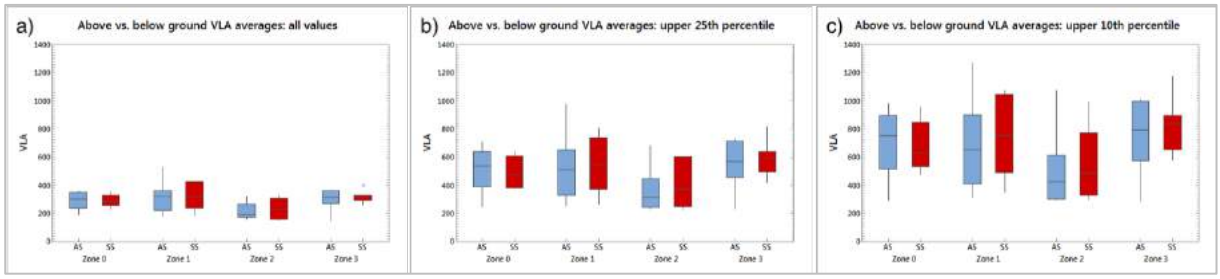

Figure 32: Comparison of above and below ground VLA of all zones: a) all values, b) upper 25th percentile of all values, c) upper 10th percentile of all values.

Differences in VLA in above and below ground VLA showed no significant in any of the zones. (Table 10).

Table 10: Result overview of T-test (T-value) comparing VLA from above (AS) and below ground (SS) with DF (Degrees of freedom).

		Z_0	**Z_1**	**Z_2**	**Z_3**
All samples	*T*-value	0.09	-0.14	-0.59	-0.63
	DF	16	17	11	10
	p	0.9313	0.8907	0.5665	0.5428
Upper 25th percentile	*T*-value	0.27	-0.27	-0.5	-0.46
	DF	16	17	11	12
	p	0.7904	0.7916	0.6239	0.6548
Upper 10th percentile	*T*-value	0.11	-0.49	-0.42	-0.57
	DF	16	17	11	12
	p	0.9129	0.6285	0.6796	0.5805

5.4.3 VLA Zone average (Z_0-Z_3) (Global measurements)

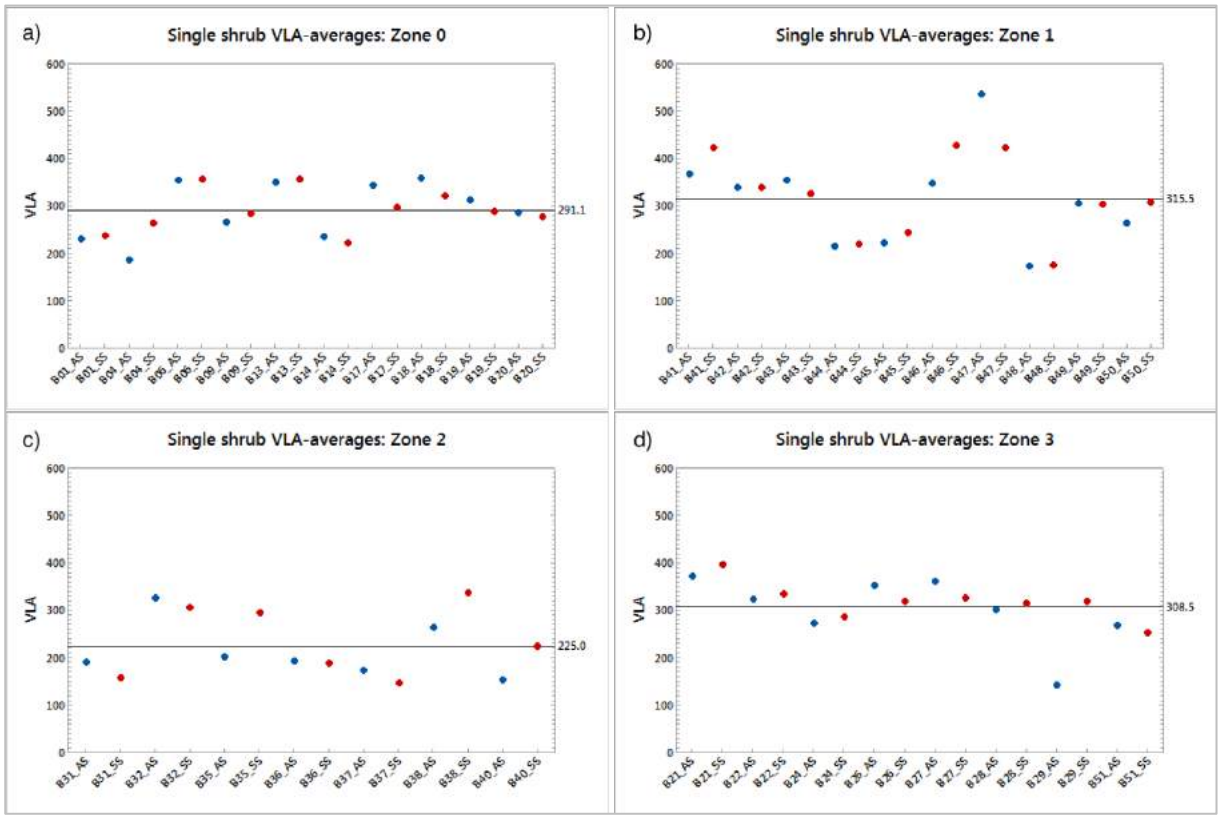

Figure 33: Dot plot of VLA averages including mean zonal average (black line) of: a) Z_0, b) Z_1, c) Z_2 and d) Z_3.

For the comparison of average vessel lumen area of each zone the following sample size was used [n_{Z0}=20, n_{Z1}=20, n_{Z2}=14, n_{Z3}=16] including both above ground samples (blue dots) and below ground samples (red dots) (Figure 33a-d).

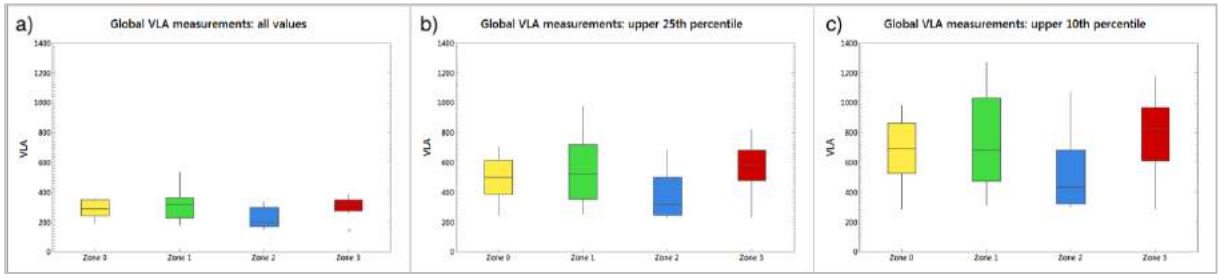

Figure 34: Boxplots of zone VLA averages with indication of variance between all zones: a) all values, b) upper 25th percentile and c) upper 10th percentile.

The comparison of all measured vessels from each zone showed that Z_0, Z_1 and Z_3 shared similar VLA sizes, whilst Z_2 was smaller ($F_3 = 5.17$, $p = 0.0029$). This is evident in Figure 33, where $Z_0 = 291.1$ µm^2, $Z_1 = 315.5$ µm^2 and $Z_3 = 308.5$ µm^2) whilst for Z_2 a substantially smaller VLA was found (225.0 µm^2), representing a difference of ≥66.6 µm^2 compared to the other zones. The greatest variance in VLA measurements was found for Z_1 (SD = 93.58 µm^2), while in the other zones the variance is lower (Z_0 = 52.47 µm^2, Z_2 = 67.37 µm^2 and Z_3 = 58.96 µm^2) (Figure 34a).

Comparing the upper 25th percentile of measured vessels with ANOVA also indicates a significant difference in vessel sizes of at least one zone ($F_3 = 3.94$, $p = 0.0119$). The following Tukey-Kramer test grouped the averages into group A (Z_0, Z_1 and Z_3) and group B (Z_0 and Z_2) indicating that the average VLA in Z_2 is significantly different (lower) to Z_1 and Z_3 but similar if compared to Z_0. The variance of the means again differs in Z_1 (SD = 201.5 µm^2), being higher than the variances in the other zones (Z_0 = 126.45 µm^2, Z_2 = 155.32 µm^2 and Z_3 = 143.89 µm^2) (Figure 34b).

In the comparison of the upper 10th percentile ANOVA indicates a significant difference in average VLA of at least one zone as well ($F_3 = 2.90$, $p = 0.0415$), but this outcome is still less significant than the other two test results. The following Tukey-Kramer test grouped the averages into group A (Z_0, Z_1 and Z_3) and group B (Z_0, Z_1 and Z_2) only indicating a statistical difference between the means of Z_2 and Z_3. The variance of the means is the highest in Z_1 (SD = 288.26 µm^2) while the variances in the other zones are (Z_0 = 196.96 µm^2, Z_2 = 256.00 µm^2 and Z_3 = 219.98 µm^2) (Figure 34c).

5.5 Climate data

5.5.1 Temperature (DMI vs. KNMI)

The summer temperatures of the two datasets (DMI and KNMI) were plotted and compared for the growing season (June, July, August) and showed a significant correlation ($r_s = 0.74$, $p < 0.0001$) for the period 1977-2017 (Figure 35). The long-term averages of the growing season temperature derived from Ilulissat meteorological station and the KNMI gridded dataset are 6.80 °C respectively 5.54 °C.

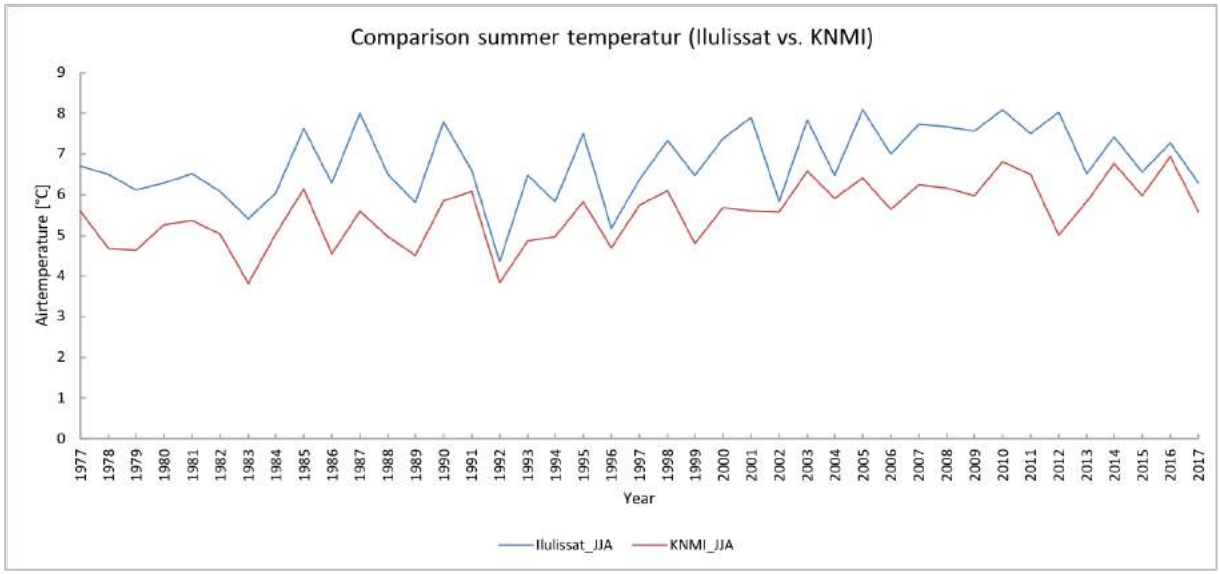

Figure 35: Comparison of summer temperatures from Ilulissat weather station and the gridded KNMI temperature dataset for June, July and August.

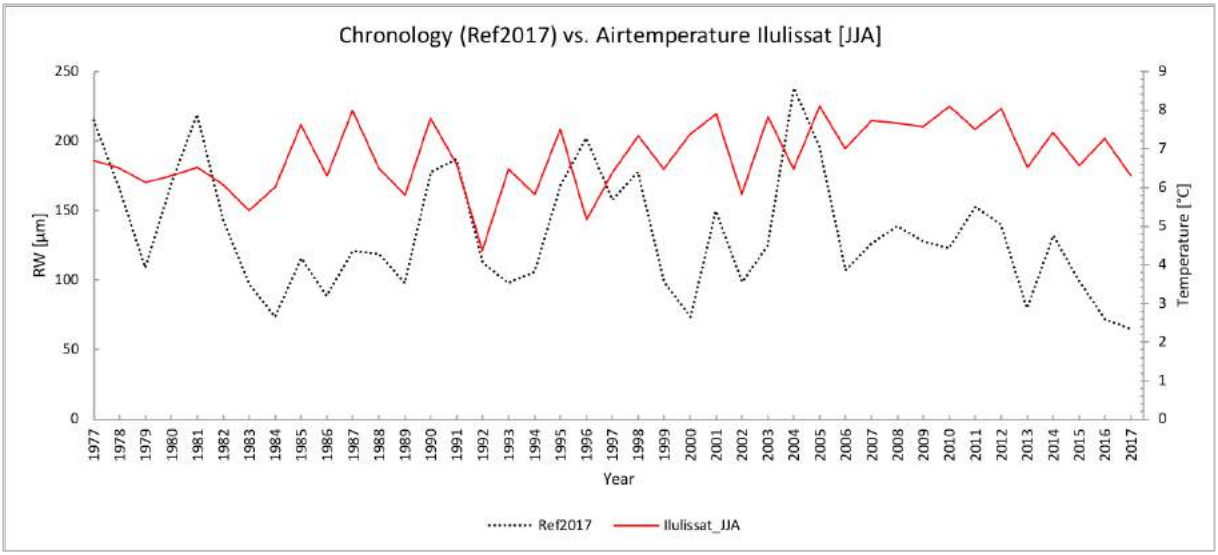

Figure 36: Betula chronology (Ref2017) vs. summer temperatures from June, July and August averaged from the DMI dataset from Ilulissat meteo station.

The reference chronology was compared to the summer temperature curve from the DMI dataset, (Figure 36) and showed no significant correlation ($r_s = 0.141392$, $p = 0.3779$). As the two temperature datasets from DMI and KNMI correlate on a high level ($r_s = 0.74$, $p < 0.0001$), the correlation to Ref2017 was only tested for the DMI dataset and no significant correlation with the KNMI dataset was assumed.

Table 11: Results from correlation analysis of single month temperature averages and seasonal temperature combination to chronology Ref2017.

Same year			previous year	
Single month averages	***p*-value**	***Correlation coefficient***	***p*-value**	***Correlation coefficient***
May	0.067	0.289313	0.287	-0.17257
June	0.286	0.170772	0.225	-0.19640
July	0.817	0.037350	0.190	-0.21147
August	0.711	0.059677	0.166	-0.22322
September	0.957	-0.008722	0.339	-0.15520
Seasonal combinations				
Jun/Jul	0.345	0.151408	0.112	-0.25503
Aug/Sep	0.860	0.028398	0.151	-0.23158
May/Jun	0.074	0.281664	0.185	-0.21405
Jan/Feb/Mar	0.218	0.196403	0.758	0.05021
Apr/May/Jun	0.254	0.182415	0.450	-0.12281
Jul/Aug	0.7178	0.058191	0.106	-0.259663
Apr/May	0.3378	0.153559	0.645	-0.075088
Jun/Jul/Aug	0.3779	0.141392	0.072	-0.287112
Jul/Aug/Sep	0.8137	0.037966	0.089	-0.272589
May/Jun/Jul	0.0894	0.268697	0.109	-0.257667
Jun-Sep	0.4937	0.109955	0.068	-0.291728
May-Sep	0.1919	0.208004	0.076	-0.283923

The temperature was then tested for correlation with Ref2017 in a row of seasonal both from the same growth year and previous growth year (Table 11). None of the single months or seasonal combinations correlated with the reference chronology, before and during the growing season.

5.5.2 Ground temperatures

Three seasonal cycles are apparent over the whole measured period with the soil being unfrozen during the month July, August and September. Thawing of the ground starts at the end of May and the freezing takes place during October (Figure 37).

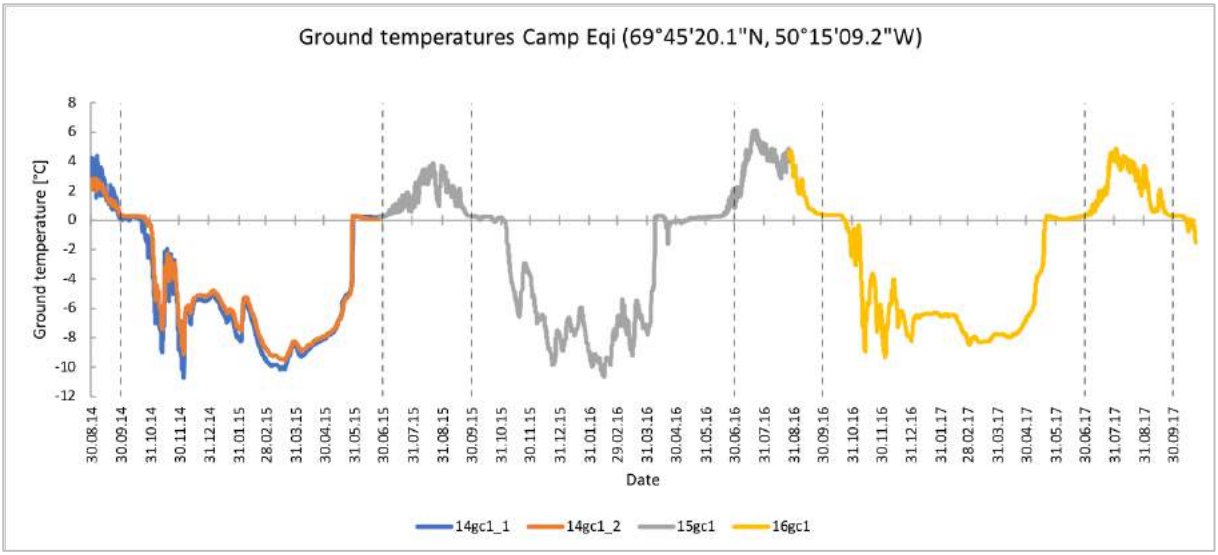

Figure 37: Seasonal soil temperature cycles from 2014 to 2017. Dashed lines indicate the growing season July-September.

5.5.3 Precipitation

Growing season (GS) and non-growing season (NGS) precipitation totals of each year were tested for correlation with the reference chronology (Ref2017). The total GS precipitation (July–September) does not correlate with the chronology (r_s = -0.044, p = 0.783) and neither does the NGS (r_s = 0.071, p = 0.659).

5.6 Spatiotemporal reconstruction of single tsunami event years

Disturbance years of the four major events which affected ≥5 specimens, elaborated in chapter 5.3.1 (Table 7). The events were visualised on a map as affected shrubs for the incidents in 1997, 2002, 2006 and 2013 were singled out individually for each year. The reach of the tsunami disturbances across Z_1 to Z_3 differ for each of the event years. Some shrubs showed disturbances in up to 3 of the four event years (B24_3d) and were therefore visualised for each event (Figure 38).

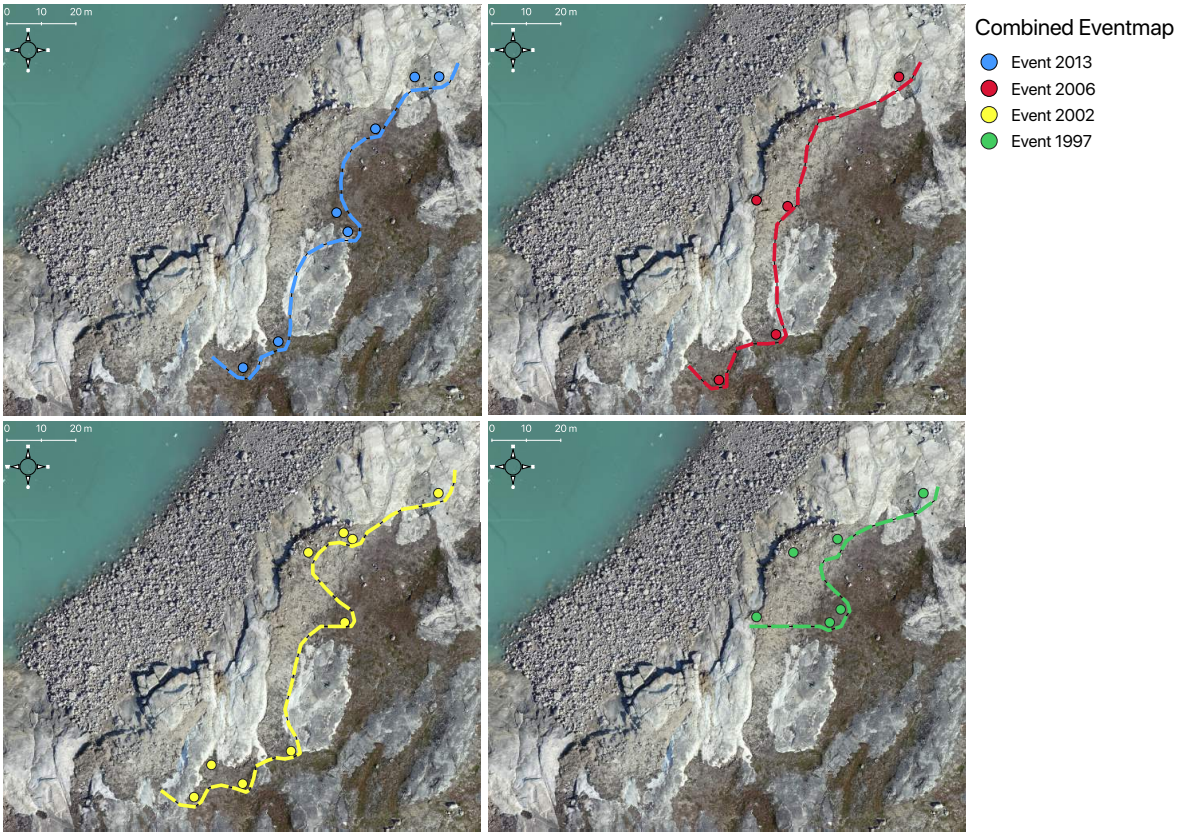

Figure 38: Combined event map of years 2013, 2006, 2002 and 1997.

6 Discussion

6.1 Tsunami effect on shrub growth

Several of the more recent tsunami events at Eqip Sermia have mainly been documented by Lüthi et al., (2016). The documented recent retreat of the Eqip Sermia outlet glaciers, described tsunami activity and the height of the ice cliff at the glacier front were summarized in Table 12. Tsunamis with a runup of 15-20 m have been described as from the year 2012 onward.

Table 12: Summary of documented glacier-induced tsunami activity of Eqip Sermia outlet glacier, with estimated heights of the ice cliff at the glacier front.

Year	Event description	height of ice cliff	Source
2000	Onset of retreat	<100 m (assumed)	(Lüthi et al. 2016)
2001	retreat	<100 m (assumed)	(Lüthi et al. 2016)
2002	retreat	<100 m (assumed)	(Lüthi et al. 2016)
2003	Pause of retreat	<100 m (assumed)	(Lüthi et al. 2016)
2004		<100 m (assumed)	(Lüthi et al. 2016)
2005		<100 m (assumed)	(Lüthi et al. 2016)
2006		<100 m (assumed)	(Lüthi et al. 2016)
2007		<100 m (assumed)	(Lüthi et al. 2016)
2008		<100 m (assumed)	(Lüthi et al. 2016)
2009	northern lobe retreats (1.5 km in one year)	<100 m (assumed)	(Lüthi et al. 2016)
2010	Start of the latest retreat	<100 m (assumed)	(Lüthi et al. 2016)
2011		100-150 m	(Lüthi et al. 2016)
2012	start of the formation of big ice cliff at glacier front, start of tsunamis with runup of 15-20 m	150-200 m	(Lüthi et al. 2016)
2013	southern lobe retreats (1 km in one year), tsunamis with runup of 15-20 m (single event captured on video)	150-220 m	(Lüthi et al. 2016) (Lüthi & Vieli 2016)
2014	central front is resting on shallow bedrock, July 2 collapse front (big event)	200 m	(Lüthi et al. 2016) (Lüthi & Vieli 2016)
2015		200 m	(Lüthi et al. 2016)

The annual ring width measurements of suspected tsunami affected shrubs were compared with an unaffected reference chronology. It was found that in the year 2013 multiple specimens of tsunami affected zones showed decreased ring growth while the reference chronology indicates an increase of growth in the same year (Figure 25 & 26). For the same year Lüthi et al. (2016) describe the glacier front of Eqip Sermia as geometrically favourable for the occurrence of large glacier-induced tsunamis with a steep and high ice cliff which developed in the central northern part of the glacier. In 2013 this massive ice cliff likely reached its maximum height of 150-220 m, enabling wave runups on the opposite shore of 15-20 m, depending on the geometry of the shoreline (Lüthi et al. 2016). Within the study area, the zones Z_1 to Z_3 were located on elevations between 8 m and 11 m a.s.l. (Figure 10), well within the reach of tsunami activity. In 2013, a glacier-induced tsunami destroyed the boat-landing of a local tour operator which was caught on camera (www.youtube.com; Lüthi & Vieli 2016). The ring width measurements of the year 2013 suggest that this, or a similar tsunami was likely responsible for the observed growth limitations, visible in shrubs sampled in Z_1 to Z_3 (Figure 26), which are visible in form of decreased ring growth in comparison with the reference (Figure 25).

Shrubs growing under conditions of suspected low tsunami influence (Z_1) and intermediate tsunami influence (Z_2) were shown to have a stronger positive correlation to the reference chronology than shrubs growing under strong tsunami influence (Z_3) (Table 3, 4, 5). The average correlation coefficient of significantly correlating specimens in Z_1 is 0.202 higher than in Z_3 and the one in Z_2 is 0.187 higher respectively. This suggests that the growth response of shrubs influenced by glacier-induced tsunamis is different from the growth response of unaffected specimens or of specimens growing under low tsunami influence. These reductions in growth altering effects may be induced by the effects of saltwater intrusion into the soil and associated increase in soil salinity, which has been shown to cause a reduction in ring growth (e.g. Lopez Caceres et al. 2018). Increased soil salinity or saltwater intrusion are known to have limiting effects on tree and shrub growth because of stomatal closure due to salinity stress (Munns 2002; Lopez Caceres et al. 2018). Plant physiological responses to water stress (insufficient for plant growth) are similar to stress-induced by increased soil salinity since it reduces the water availability for the plants (Munns 2002; Tombesi et al. 2015). Despite the lack of a significant difference in average ring width between shrubs from tsunami affected and unaffected zones, the growth variability in Z_3 was considerably lower than in the reference zone by a difference of 18.13 µm (Figure 22). This indicates a zonal growth suppression of shrubs within the area susceptible to strong tsunami influence with associated growth limitations. This notion is supported by Boudreau & Villeneuve-Simard (2012) who documented shrub growth reduction, along with lower variability in annual growth, of suppressed shrubs than in specimens growing in optimum conditions.

Little evidence was found in the analysis of growth disturbances that suggested glacier-induced tsunamis were responsible for mechanical damage to the plants. Only two specimens showed indications of callus tissue in response to an earlier injury and only three plants displayed signs of reaction wood (Table 6). However, none of the plants growing in the zone with strong tsunami influence (Z_3) showed any signs of wood anatomical reaction to mechanical damage and in the known tsunami year 2013 no disturbance was found at all. Therefore, it can be assumed that mechanical damages were caused by processes other

than tsunami activity. This is supported by the findings of Buchwal et al. (2015), who found that cambial injuries could be related to solifluction processes which are predominant in permafrost terrains, as they are able to induce slow mechanical stress on rooting plants. Solifluction refers to a slow downwards moving slope in connection to freeze-thaw cycles and saturated soils in cold environments (Matsuoka 2001). However, the study site shows no indication of landforms typical for regular solifluction activity, such as distinct lobes or stripes as described by Matsuoka (2001).

According to Lopez Caceres et al. (2018) trees can react to saltwater stress with decreased ring growth, and that the size of plant vessels are similarly affected by saltwater stress, since they are responsible for the water transport within the plant. However, there was no significant correlation between VLA and ring growth (annual VLA reference of Z_0 to the reference chronology). Despite this, there are indications that in the years 2000 and 2005 multiple shrubs showed decreasing VLA compared to the VLA reference (Figure 29). They are in no direct relation to growth reactions noted in ring width (Figure 26).
Global VLA measurements of every plant suggest that a general negative reaction exists in response to increased salt stress-induced by glacier-induced tsunamis. The average VLA in Z_2 is significantly smaller than the average VLA of the Z_0 (Figure 32 & 33). In the Z_2 (intermediate tsunami influence) the majority of the sampled shrubs showed recovery from tsunami inundation yet showing signs of stress with notably less leaf growth than shrubs sampled in the reference zone. Since the average VLA in shrubs susceptible to high tsunami influence is not different to the reference VLA it can be assumed that shrubs growing under strong tsunami influence did not have the possibility to recover from recent increasing tsunami activity described by Lüthi et al. (2016) and more likely died rather than recovered from the damage. The effect of a shrub dieback is visible in Figure 10, were evidently more than 70 % of the deceased shrubs died after the year 2012, consistent with the year where an increase in tsunami activity was observed at Eqip Sermia (Table 12). This dieback of shrubs exposed to salt stress after flooding is consistent with the findings of Lantz et al. (2015).

6.2 Event years and reach of tsunami

Based on the findings that glacier-induced tsunamis have a negative impact on vegetation in disturbed areas through limiting annual ring growth it should be possible to reconstruct past tsunami activity in the scope of this study. The nature of glacier-induced tsunamis does not allow us to reconstruct single tsunami events, rather reconstruct event years of assumed increased tsunami activity. However, the documented single tsunami event of 2013 in Lüthi & Vieli (2016) likely had the capability of affecting shrub growth and induced growth limitations, visible within our samples in the year 2013. As archives about tsunami activity in the past are incomplete, a reconstruction of further event years of increased tsunami activity was attempted.
The incident of 2013 (Lüthi & Vieli 2016) affected a total of 7 plants in the study area and two specimens in Z_3 showed simultaneous decreases in growth. A total of 6 more incidents were noted during the past four decades, where multiple specimens from different zones display decreased ring growth compared

to the reference chronology (Figure 26). In every case at least two shrubs sampled in Z_3 showed reduced growth similar to those found for the year 2013. Therefore, it is possible that further tsunami activity occurred in the years 1979, 1984, 1989, 1997, 2002 and 2006. This finding is consistent with literature as tsunamis have been described not exclusively as a recent phenomenon (Bauer cited in (Lüthi & Vieli 2016)). Lüthi et al. (2016) describe tsunami runup heights of 15-20 m to be a more recent phenomenon linked to increased frontal heights of Eqip Sermia glacier. Parts of the study area, however, are located 8 m to 11 m a.s.l. and as such the effects of smaller tsunami events would be visible in this area, supporting the reconstructed dates of event years (Figure 10).

It is possible to map the spatial extent of tsunami activity for every year by visualizing all the shrubs showing growth disturbances for that year (Figure 38). The spatial extent of the 2013 tsunami was likely the biggest of all the reconstructed events. Tsunami activity occurring in the year 2006 did not affect as many plants and was smaller in its spatial extent. The mapping suggests that calving events in 1997 and 2002 had similar spatial reach in terms of effected vegetation as the recent tsunami in 2013, as multiple specimen show growth limitations in these years. In both years, shrubs in Z_3 were highly affected with 43-57 % of the specimens in Z_3 showing limited growth during these two event years (Figure 26). A relatively smaller spatial extent for tsunami activity of the reconstructed event years 1979, 1984 and 1989 suggest that less calving activity occurred during these years and growth limiting effects on vegetation were likely confined to Z_3. Lüthi et al. (2016) and Lüthi & Vieli (2016) suggest that large glacier-induced tsunamis are a more recent phenomenon, and before the latest glacier retreats, smaller tsunami waves were caused by Eqip Sermia which attained smaller front heights throughout its documented history. This suggests that the findings above are plausible since the spatial extent of tsunami activity appears to be smaller in the earlier events of 1979, 1984 and 1989 than for the recently reconstructed events.

A temporal pattern in the disturbances induced by tsunami activity can be discerned when observing the reconstructed event years in (Figure 26 & 27). The smaller events occurring before 1997 suggest that the extent of calving-induced tsunami activity follows the description of Bauer (cited in Lüthi & Vieli (2016)). After Eqip Sermia began its recent retreats (Table 12), accompanied by higher calving rates, tsunami activity increased in frequency and magnitude (Figure 26). It is suggested by Lüthi et al. (2016) that tsunamis of high magnitudes with wave runups of 15-20 m coincide with the formation of an ice cliff at the glacier front. This is supported by the data that disturbances were noted in the years 2012 to the current day (Figure 26). High tsunami activity, leading to more frequent saltwater intrusion into the soil, not only limits plant growth (Lopez Caceres et al. 2018), it can lead to a dieback of the affected vegetation (Lantz et al. 2015). The mortality years of sampled shrubs (Figure 30) suggest an increased dieback of shrub vegetation from 2012 to 2017 with more than 70 % of deceased plants killed during this period. Limited shrub growth thus appears to coincide with an increased dieback of vegetation caused by tsunami activity. The mortality years of dated samples also occurs concurrently with

vegetation dieback and increase of soil erosion and appears to be related to the formation of the ice cliff in the central sector of the glacier front (Lüthi et al. 2016).

Further retreat of the Eqip Sermia calving front is likely to occur based on the current conditions of the glacier (Lüthi & Vieli 2016). As the central sector of the glacier front attains heights of 150-200 m, future glacier-induced tsunami activity can be expected but is not likely to significantly increase, since the maximum height of the ice cliff was reached in 2013 and has been decreasing slightly since then (Lüthi et al. 2016). The long-term development of the frontal glacier position is more difficult to predict as Lüthi & Vieli (2016) suggest that the glacier front may possibly recede into an over-deepened basin which would likely cause a decrease in the frontal height of the glacier, with an associated reduction in tsunami activity. A further retreat of the ablation front would mean that the study area will no long directly face the glacier front and thus only indirect effects of tsunamis would be expected in this area (Figure 10). However, glacier-induced tsunamis would still be expected to impact other parts of the fjord, and as Camp Eqi is located further west with more direct exposure to the calving front, tsunamis can still be expected to affect and shape the shores of that area in the years to come.

6.3 Growth reaction to climate

Considerable annual variations in radial growth specimens (Figure 21a), unaffected by tsunami activity, suggest that radial growth variations are induced by changing climatic conditions, such as changes in local air temperature and precipitation. A positive correlation of *Betula nana* growth to both increasing summer and winter temperatures has been shown by Hollesen et al. (2015) in a comparable study of Disko island in West Greenland. A comparable growth reaction to air temperatures was expected for the sampled shrubs of the reference area (Z_0) when being compared to a regional air temperature dataset. However, shrub growth of samples in the scope of this study does not positively correlate with regional air temperatures. As ground temperature records only span a period of three years, they are too short to provide substantial proof of correlation to shrub growth. Nevertheless, they provide information about the local growing season in terms of the timing of soil freezing and thawing (Figure 37). Arguably, this data would have been a better estimation of local temperature at the study area than the regional available dataset, due to the relatively short time series this remains equivocal.

Shrub growth does not correlate with total monthly precipitation estimates of the region. Water availability is a crucial limiting factor for shrub growth since the climate in West Greenland is relatively dry with annual precipitation for Ilulissat to be 280 mm per year (Figure 9). Thus, annual precipitation does not appear to be the main source of water availability for shrub growth, since no correlation to annual growth could be found. It is suggested by Bhatt et al. (2017) that seasonal melt water availability contributes considerably to the total water availability necessary for vegetation growth. Seasonal melt water availability largely depends on snowfall during the winter months. However, it was not possible to estimate seasonal meltwater availability definitively, as neither regional nor local records of snowfall are available for the study area, and wind drift of snow may have a large influence on the local

distribution of snow cover. Lenaerts et al. (2012) investigated the spatial variability of drifting snow in Greenland and suggest that coastal areas of the western margins of the Greenlandic ice sheet are more affected by drifting snow than the central parts of the ice sheet. However, the coarse spatial resolution of the applied model does not allow local estimations for Camp Eqi to be drawn in terms of how much snow is locally accumulated in the study area.

With no correlations between shrub growth and air temperature or climate records it can be expected, that the local microclimate is responsible for impacts on vegetation growth. Microclimatic conditions are hard to replicate, as multiple factors such as local ground temperature, soil moisture wind exposure and winter snow cover contribute to vegetation growth conditions (Wahren et al. 2005).

6.4 Error discussion

Using a dendrochronological approach on Arctic shrubs such as *Betula nana* requires a careful and thorough crossdating process. The importance of annual crossdating in order to obtain precise and reproducible results is stressed in multiple studies (e.g. Myers-Smith et al. 2015; Buchwal et al. 2015; Buchwal et al. 2013; Bär et al. 2006). Careful visual crossdating, following the procedure of Myers-Smith et al. (2015), was conducted on the sampled shrubs followed by the statistical correlation of individual shrubs to the reference and testing for significance (Table 2).

Even though individual shrubs positively correlated to the reference significantly (with the exception of B13_0a) a certain level of uncertainty remains in the crossdating process as missing or partially missing rings are hard to detect and remain a potential source of error. Multiple ring width radii measurements were conducted on each sample to minimise the level of uncertainty. However potential human errors cannot be totally eliminated. The level of uncertainty remains in the proceeding analyses as the reference chronology was the basis for dating deceased specimens in Z_3, detecting glacier-induced tsunami disturbances and dating annual VLA measurements. Although the source of crossdating uncertainty cannot be completely eliminated, carefully conducted crossdating and significant correlation of individual shrubs composing the chronology, suggest obtained results are correct.

A second potential source of error was the obtained measurement of the last growth ring of 2018. In some cases, it was hard to determine whether ring growth had already begun or not, since some plants had already started forming a ring for year 2018 and some had not. Especially for narrow rings in outer parts of the plants, it was potentially hard to determine if ring growth had already initialised. For specimens in Z_3, multiple levels of decay could be observed, as the deceased shrubs were dated to more than 10 years ago. However, dry and stable conditions, due to low precipitation and cold temperatures, slowed down wood decay considerably and therefore measurements of ring width and VLA of partially decayed plants were still possible. However, in some cases advanced decay made it nearly impossible to obtain accurate results. The shrubs in question were excluded from the analysis in order to eliminate this potential source of error.

7 Conclusion

Large glacier-induced tsunamis are caused by calving processes of marine-terminating outlet glaciers. The Eqip Sermia outlet glacier in West Greenland has been retreating for the past century and the latest retreat enabled the formation of a massive ice cliff in the frontal area, with an estimated height of 150-200 m. As a result, large calving events trigger tsunamis of unprecedented proportions, causing erosion on soil and vegetation on the slope facing the glacier front.

This thesis aimed to find, if growth limiting effects of glacier-induced tsunamis are visible in a prominent Arctic shrub species (*Betula nana*) and thus if past tsunami activity can be reconstructed using a dendrochronological approach. A reference chronology consisting of 13 crossdated samples of unaffected shrubs was constructed as a comparison. Detectable growth limitations in multiple specimens sampled in affected zones suggest, that glacier-induced tsunamis disturb ring growth of *Betula nana*. In disturbed specimens, this is visible in the form of narrower growth rings compared to the reference chronology. Arguably these growth limitations are caused from increased soil salinity rather than through mechanical damage of the plants, as growth reactions on a wood anatomical level such as callus tissue or reaction wood were missing in the majority of the sampled specimens. Growth limitations are visible in the ring structures of multiple plants and can be linked to a documented tsunami at Eqip Sermia in the year 2013.

Using the given information about the 2013 tsunami and the effects it caused on shrub growth, a reconstruction of 6 more event years with increased tsunami activity was attempted for the period of 1977 to 2017. It appears that glacier-induced tsunamis have increased in size, since the turn of the century, more shrubs showed growth limitations for the same years and the spatial distribution of the affected shrubs increased. A dieback of plants starting in 2012 coincides with the formation of an ice cliff at the central sector of the Eqip Sermia calving front. This is supported by literature describing massive tsunamis with a wave runup of 15-20 m a.s.l. to be a rather recent phenomenon. No significant correlations between shrub growth and regional temperature and precipitation was found in the scope of this study, with other microclimatic factors such as snow cover, soil moisture and soil temperature potentially influencing vegetation growth on a local level.

The precise crossdating of all attained samples posed the biggest challenge of this thesis. Even though the opinion of a second person was used to verify the quality of the crossdating process a certain level of subjectivity and uncertainty remains. As most of the results of this thesis depend on a properly crossdated chronology, this step was conducted with greatest care. Nevertheless, to account for the existence of missing and partially missing rings was unavoidable, as they regularly occur in Arctic tundra shrubs species.

This thesis provides an important base for understanding the influence of glacier-induced tsunamis on Arctic shrubs growth and the suitability of *Betula nana* as a potential archive for past tsunami activity. Further research is needed however, on the precise cause of growth limitations induced by tsunami waves and whether a single event is capable of causing growth limitations, rather than multiple events occurring in the same growth season. This information could be useful in order to determine if growth

limitations induced by glacier-induced tsunamis can be used to date historical changes in the calving dynamics of a glacier or if just single events can be reconstructed. Testing other shrub species could potentially be of further values, if growth limitations are just visible in *Betula nana* shrubs or if they can be found in further species, possibly with more prominent disturbances.

As Eqip Sermia glacier is likely to retreat further in the near future as a result of increased global warming and associated glacier calving, the phenomenon of glacier-induced tsunamis should be subject of further investigations. Such research will be crucial in assessing the potential danger these events pose to inhabited areas and infrastructure.

8 Literature

Alestalo, J., 1971. Dendrochronological interpretations of geomorphic processes. *Fennia*, 105, pp.1–139.

Allen, M.R., O.P. Dube, W. Solecki, F. Aragón-Durand, W. Cramer, S. Humphreys, M. Kainuma, J. Kala, N. Mahowald, Y. Mulugetta, R. Perez, M. Wairiu, and K. Zickfeld, 2018: Framing and Context. In: Global Warming of 1.5°C. An IPCC Special Report on the impacts of global warming of 1.5°C above pre-industrial levels and related global greenhouse gas emission pathways, in the context of strengthening the global response to the threat of climate change, sustainable development, and efforts to eradicate poverty [Masson-Delmotte, V., P. Zhai, H.-O. Pörtner, D. Roberts, J. Skea, P.R. Shukla, A. Pirani, W. Moufouma-Okia, C. Péan, R. Pidcock, S. Connors, J.B.R. Matthews, Y. Chen, X. Zhou, M.I. Gomis, E. Lonnoy, T. Maycock, M. Tignor, and T. Waterfield (eds.)]. In Press.

Amundson, J.M. et al., 2008. Glacier, fjord, and seismic response to recent large calving events, Jakobshavn Isbræ, Greenland. *Geophysical Research Letters*, 35(22), pp.2–6.

Amundson, J.M. et al., 2010. Ice mélange dynamics and implications for terminus stability, Jakobshavn Isbrse, Greenland. *Journal of Geophysical Research: Earth Surface*, 115(1), pp.1–12.

Bär, A., Bräuning, A. & Löffler, J., 2006. Dendroecology of dwarf shrubs in the high mountains of Norway - A methodological approach. *Dendrochronologia*, 24(1), pp.17–27.

Benn, D.I. et al., 2017. Glacier Calving in Greenland. *Current Climate Change Reports*, 3(4), pp.282–290.

Benn, D.I., Warren, C.R. & Mottram, R.H., 2007. Calving processes and the dynamics of calving glaciers. *Earth-Science Reviews*, 82(3–4), pp.143–179.

Berz, G. et al., 2001. World Map of Natural Hazards, 3rd edition. *Natural Hazards*, 23, pp.443–465.

Bhatt, U.S. et al., 2017. Changing seasonality of panarctic tundra vegetation in relationship to climatic variables. *Environmental Research Letters*, 12(5).

Boudreau, S. & Villeneuve-Simard, M.-P., 2012. Dendrochronological evidence of shrub growth suppression by trees in a subarctic lichen woodland. *Botany*, 90(2), pp.151–156.

Box, J.E. et al., 2019. Key indicators of Arctic climate change: 1971–2017. *Environmental Research Letters*, 14(4), p.045010. Available at: http://stacks.iop.org/1748-9326/14/i=4/a=045010?key=crossref.dc1379b707c0d2efabafd34a096a37d5.

Box, J.E. & Decker, D.T., 2011. Greenland marine-terminating glacier area changes: 2000-2010. *Annals of Glaciology*, 52(59), pp.91–98.

Brown, C.S., Meier, M.F. & Post, A., 1982. Calving Speed of Alaska Tidewater Glaciers, With Application to Columbia Glacier. *U.S. Geological Survey Professional Paper*, 1258–C, pp.1–13.

Buchwal, A. et al., 2015. New insights into the 21 November 2000 tsunami in West Greenland from analyses of the tree−ring structure of Salix glauca. *Polish Polar Research*, 36(1), pp.51–65.

Buchwal, A. et al., 2013. Temperature modulates intra-plant growth of Salix polaris from a high

Arctic site (Svalbard). *Polar Biology*, 36(9), pp.1305–1318.

Cappelen, J., 2018. *DMI Report 18-04 Greenland - DMI Historical Climate Data Collection 1784-2017*, Available at: http://www.dmi.dk/laer-om/generelt/dmi-publikationer/Url:http://www.dmi.dk/laer-om/generelt/dmi-publikationer/Website:www.dmi.dk.

Chartier, M.P., Rostagno, C.M. & Roig, F.A., 2009. Soil erosion rates in rangelands of northeastern Patagonia: A dendrogeomorphological analysis using exposed shrub roots. *Geomorphology*, 106(3–4), pp.344–351. Available at: http://dx.doi.org/10.1016/j.geomorph.2008.11.015.

Eidesen, P.B., Alsos, I.G. & Brochmann, C., 2015. Comparative analyses of plastid and AFLP data suggest different colonization history and asymmetric hybridization between Betula pubescens and B. nana. *Molecular Ecology*, 24(15), pp.3993–4009.

Enderlin, E.M. et al., 2014. An improved mass budget for the Greenland ice sheet. *Geophysical Prospecting*, 41(9), pp.3307–3314.

Fritz, H.M., Hager, W.H. & Minor, H.E., 2003. Landslide generated impulse waves. 1. Instantaneous flow fields. *Experiments in Fluids*, 35(6), pp.505–519.

Garrett, C. & Munk, W., 2001. Landslide tsunami. *Journal of Geophysical Research*, 106(6), pp.201–211.

Gärtner-Roer, I., Heinrich, I. & Gärtner, H., 2013. Wood anatomical analysis of Swiss willow (Salix helvetica) shrubs growing on creeping mountain permafrost. *Dendrochronologia*, 31(2), pp.97–104. Available at: http://dx.doi.org/10.1016/j.dendro.2012.09.003.

Gärtner, H. et al., 2015. A Technical Perspective in Modern Tree-ring Research - How to Overcome Dendroecological and Wood Anatomical Challanges. *Jove journal of visualized experiments*, 97.

Gärtner, H., 2007. Tree roots - Methodological review and new development in dating and quantifying erosive processes. *Geomorphology*, 86(3–4), pp.243–251.

Gärtner, H., Lucchinetti, S. & Schweingruber, F.H., 2015. A new sledge microtome to combine wood anatomy and tree-ring ecology. *IAWA Journal*, 36(4), pp.452–459.

Gärtner, H. & Schweingruber, F.H., 2013. *Microscopic preparation techniques for plant stem analysis*, Verlag Dr. Kessel.

Gärtner, H., Schweingruber, F.H. & Dikau, R., 2001. Determination of erosion rates by analyzing structural changes in the growth pattern of exposed roots. *Dendrochronologia*, 19(1), pp.81–91.

Gers, E. et al., 2001. Application of shrubs for dendrogeomorphological analysis to reconstruct spatial and temporal landslide movement patterns. A preliminary study. *Zeitschrift für Geomorphologie Supplementband*, 125, pp.163–175.

De Groot, W.J., Thomas, P.A. & Wein, R.W., 1997. Betula nana L. and Betula glandulosa Michx. *Journal of Ecology*, 85, pp.241–264.

Hellberg, E. & Carcaillet, C., 2003. Wood anatomy of West European Betula: Quantitative descriptions and applications for routine identification in paleoecological studies. *Ecoscience*, 10(3), pp.370–379.

Higgins, A.K., 1991. North Greenland Glacier Velocities and Calf lce Production. *Polarfoorschung*, 60(July), pp.1–23.

Hoelzle, M. et al., 2014. Global Land Ice Measurements from Space. , (July). Available at: http://link.springer.com/10.1007/978-3-540-79818-7.

Hollesen, J. et al., 2015. Winter warming as an important co-driver for Betula nana growth in western Greenland during the past century. *Global Change Biology*, 21(6), pp.2410–2423.

Howat, I.M. et al., 2010. Seasonal variability in the dynamics of marine-terminating outlet glaciers in Greenland. *Journal of Glaciology*, 56(198), pp.601–613.

Hulten, E., 1968. *Flora of Alaska and Neighboring Territories; a Manual of the Vascular Plants.*, Stanford, California: Stanford University Press.

IPCC, 2013: Summary for Policymakers. In: Climate Change 2013: The Physical Science Basis. Contribution of Working Group I to the Fifth Assessment Report of the Intergovernmental Panel on Climate Change [Stocker, T.F., D. Qin, G.-K. Plattner, M. Tignor, S.K. Allen, J. Boschung, A. Nauels, Y. Xia, V. Bex and P.M. Midgley (eds.)]. Cambridge University Press, Cambridge, United Kingdom and New York, NY, USA.

IPCC, 2018: Summary for Policymakers. In: Global Warming of 1.5°C. An IPCC Special Report on the impacts of global warming of 1.5°C above pre-industrial levels and related global greenhouse gas emission pathways, in the context of strengthening the global response to the threat of climate change, sustainable development, and efforts to eradicate poverty [Masson-Delmotte, V., P. Zhai, H.-O. Pörtner, D. Roberts, J. Skea, P.R. Shukla, A. Pirani, W. Moufouma-Okia, C. Péan, R. Pidcock, S. Connors, J.B.R. Matthews, Y. Chen, X. Zhou, M.I. Gomis, E. Lonnoy, T. Maycock, M. Tignor, and T. Waterfield (eds.)]. World Meteorological Organization, Geneva, Switzerland, 32 pp.

IPCC, 2014: Summary for policymakers. In: Climate Change 2014: Impacts, Adaptation, and Vulnerability. Part A: Global and Sectoral Aspects. Contribution of Working Group II to the Fifth Assessment Report of the Intergovernmental Panel on Climate Change [Field, C.B., V.R. Barros, D.J. Dokken, K.J. Mach, M.D. Mastrandrea, T.E. Bilir, M. Chatterjee, K.L. Ebi, Y.O. Estrada, R.C. Genova, B. Girma, E.S. Kissel, A.N. Levy, S. MacCracken, P.R. Mastrandrea, and L.L. White (eds.)]. Cambridge University Press, Cambridge, United Kingdom and New York, NY, USA, pp. 1-32.

Jacobs, S.S. et al., 1992. Melting of ice shelves and the mass balance of Antarctica. *Journal of Glaciology*, 38(130).

Joughin, I. et al., 2008. Ice-front variation and tidewater behavior on Helheim and Kangerdlugssuaq Glaciers, Greenland. *Journal of Geophysical Research: Earth Surface*, 113(1), pp.1–11.

Kaennel, M. & Schweingruber, F.H., 1995. *Multilingual glossary of dendrochronology*, Paul Haupt Publishers Berne Stuttgart Vienna.

Kirkbride, M.P. & Warren, C.R., 1997. Calving processes at a grounded ice cliff. *Annals of Glaciology*, (24), pp.116–121.

Lang, A. et al., 1999. Classic and new dating methods for assessing the temporal occurrence of mass movements. *Geomorphology*, 30(1–2), pp.33–52.

Lantz, T.C., Kokelj, S. V. & Fraser, R.H., 2015. Ecological recovery in an Arctic delta following

widespread saline incursion. *Ecological Applications*, 25(1), pp.172–185.

Lenaerts, J.T.M. et al., 2012. Drifting snow climate of the Greenland ice sheet: A study with a regional climate model. *Cryosphere*, 6(4), pp.891–899.

Levermann, A., 2011. When glacial giants roll over. *Nature*, (Box 1), pp.4–5.

Long, A.J., Szczuciński, W. & Lawrence, T., 2015. Sedimentary evidence for a mid-Holocene iceberg-generated tsunami in a coastal lake, west Greenland. *Arktos*, 1(1), p.6. Available at: http://link.springer.com/10.1007/s41063-015-0007-7.

Lopez Caceres, M.L. et al., 2018. Evaluation of the effect of the 2011 Tsunami on coastal forests by means of multiple isotopic analyses of tree-rings. *Isotopes in Environmental and Health Studies*, 54(5), pp.494–507.

Lüthi, M.P. et al., 2016. A century of geometry and velocity evolution at Eqip Sermia, West Greenland. *Journal of Glaciology*, 62(234), pp.640–654. Available at: https://www.cambridge.org/core/product/identifier/S0022143016000381/type/journal_article.

Lüthi, M.P. & Vieli, A., 2016. Multi-method observation and analysis of an impulse wave and tsunami caused by glacier calving. *Cryosphere*, 10(3), pp.995–1002.

Macayeal, D.R. et al., 2009. Seismic observations of glaciogenic ocean waves (micro-tsunamis) on icebergs and ice shelves. *Journal of Glaciology*, 55(190), pp.193–206.

Macayeal, D.R., Abbot, D.S. & Sergienko, O. V., 2011. Iceberg-capsize tsunamigenesis. *Annals of Glaciology*, 52(58), pp.51–56.

Machguth, H. et al., 2016. Greenland surface mass-balance observations from the ice-sheet ablation area and local glaciers. *Journal of Glaciology*, 62(235), pp.861–887.

Marzeion, B. et al., 2014. Attribution of Past Glacier Mass Loss to Anthropogenic and Natural Climate Forcing. *Science*, 345(6199), pp.919–921.

Matsuoka, N., 2001. Solifluction rates, processes and landforms: A global review. *Earth-Science Reviews*, 55(1–2), pp.107–134.

McFadden, E.M. et al., 2011. Changes in the dynamics of marine terminating outlet glaciers in west Greenland (2000-2009). *Journal of Geophysical Research: Earth Surface*, 116(2), pp.1–16.

Meier, M.F. & Post, A., 1987. Fast tidewater glaciers. *Journal of Geophysical Research*, 92(B9), pp.9051–9058.

Moon, T., Joughin, I. & Smith, B., 2015. Seasonal to multiyear variability of glacier surface velocity, terminus position, and sea ice/ice mélange in northwest Greenland. *Journal of Geophysical Research: Earth Surface*, 120, pp.159–182.

Munns, R., 2002. Comparative physiology of salt and water stress. *Plant, Cell and Environment*, 25, pp.239–250. Available at: http://dx.doi.org/10.1590/1807-1929/agriambi.v22n11p770-775.

Myers-Smith, I.H. et al., 2015. Methods for measuring arctic and alpine shrub growth: A review. *Earth-Science Reviews*, 140, pp.1–13. Available at: http://dx.doi.org/10.1016/j.earscirev.2014.10.004.

Nick, F.M. et al., 2009. Large-scale changes in Greenland outlet glacier dynamics triggered at the terminus. *Nature Geoscience*, 2(2), pp.110–114. Available at: http://dx.doi.org/10.1038/ngeo394.

Rayback, A.S.A. & Henry, G.H.R., 2005. Dendrochronological Potential of the Arctic Dwarf-Shrub Cassiope tetragona. *Tree-Ring Research*, 61(1), pp.43–53.

Rignot, E. et al., 2008. Mass balance of the Greenland ice sheet from 1958 to 2007. *Geophysical Research Letters*, 35(20), pp.1–5.

Rignot, E. & Kanagaratnam, P., 2006. Changes in the Velocity Structure of the Greenland Ice Sheet. *Science*, 311(5763), pp.986–991.

Rignot, E., Koppes, M. & Velicogna, I., 2010. Rapid submarine melting of the calving faces of West Greenland glaciers. *Nature Geoscience*, 3(3), pp.187–191. Available at: http://dx.doi.org/10.1038/ngeo765.

Roer, I., Gärtner, H. & Heinrich, I., 2007. Dendrogeomorphological analysis of alpine trees and shrubs growing on active and inactive rockglaciers. *TRACE–Tree Rings in Archaeology. Climatology and Ecology*, 5, pp.248–258.

Sargeant, C.I. & Singer, M.B., 2016. Sub-annual variability in historical water source use by Mediterranean riparian trees. *Ecohydrology*, 9(7), pp.1328–1345.

Schild, K.M. et al., 2018. Glacier Calving Rates Due to Subglacial Discharge, Fjord Circulation, and Free Convection. *Journal of Geophysical Research: Earth Surface*, 123(9), pp.2189–2204.

Schweingruber, F.H., 1990. *Anatomie europäischer Hölzer - Anatomy of European woods.*, Eidgenössische Forschungsanstalt für Wald, Schnee und Landschaft, Birmensdorf. Haupt, Bern und Stuttgart.

Shi, S. & Smith, D.E., 2003. Coastal Tsunami Geomorphological Impacts and Sedimentation Processes : Case Studies of Modern and Prehistorical Events. *Internatioal Conference on Estuaries and Coasts*, (June 2016), pp.189–198.

Shroder Jr., J.F., 1978. Dendrogeomorphological analysis of mass movement on Table Cliffs Plateau, Utah. *Quaternary Research*, 9(2), pp.168–185. Available at: http://www.sciencedirect.com/science/article/pii/0033589478900650.

Stocker, T.F., D. Qin, G.-K. Plattner, L.V. Alexander, S.K. Allen, N.L. Bindoff, F.-M. Bréon, J.A. Church, U. Cubasch, S. Emori, P. Forster, P. Friedlingstein, N. Gillett, J.M. Gregory, D.L. Hartmann, E. Jansen, B. Kirtman, R. Knutti, K. Krishna Kumar, P. Lemke, J. Marotzke, V. Masson-Delmotte, G.A. Meehl, I.I. Mokhov, S. Piao, V. Ramaswamy, D. Randall, M. Rhein, M. Rojas, C. Sabine, D. Shindell, L.D. Talley, D.G. Vaughan and S.-P. Xie, 2013: Technical Sum- mary. In: Climate Change 2013: The Physical Science Basis. Contribution of Working Group I to the Fifth Assess- ment Report of the Intergovernmental Panel on Climate Change [Stocker, T.F., D. Qin, G.-K. Plattner, M. Tignor, S.K. Allen, J. Boschung, A. Nauels, Y. Xia, V. Bex and P.M. Midgley (eds.)]. Cambridge University Press, Cambridge, United Kingdom and New York, NY, USA.

Stoffel, M., 2006. A review of studies dealing with tree rings and rockfall activity: The role of dendrogeomorphology in natural hazard research. *Natural Hazards*, 39(1), pp.51–70.

Stoffel, M. & Bollschweiler, M., 2009. What Tree Rings Can Tell About Earth-Surface Processes: Teaching the Principles of Dendrogeomorphology. *Geography Compass*, 3, pp.1013–1037.

Subarya, C. et al., 2006. Plate-boundary deformation associated with the great Sumatra-Andaman earthquake. *Nature*, 440(7080), pp.46–51.

Suni, T. et al., 2003. Interannual variability and timing of growing-season CO 2 exchange in a boreal forest. *Journal of Geophysical Research: Atmospheres*, 108(D9), p.n/a-n/a.

Tappin, D.R., Watts, P. & Grilli, S.T., 2008. The Papua New Guinea tsunami of 17 July 1998: Anatomy of a catastrophic event. *Natural Hazards and Earth System Sciences*, 8(2), pp.243–266.

Tombesi, S. et al., 2015. Stomatal closure is induced by hydraulic signals and maintained by ABA in drought-stressed grapevine. *Scientific Reports*, 5(June), pp.1–12. Available at: http://dx.doi.org/10.1038/srep12449.

Van der Veen, C.J., 2002. Calving glaciers. *Progress in Physical Geography*, 26(1), pp.96–122.

Wahren, C.H.A., Walker, M.D. & Bret-Harte, M.S., 2005. Vegetation responses in Alaskan arctic tundra after 8 years of a summer warming and winter snow manipulation experiment. *Global Change Biology*, 11(4), pp.537–552.

Walder, J.S. et al., 2003. Tsunamis generated by subaerial mass flows. *Journal of Geophysical Research: Solid Earth*, 108(B5), pp.1–19. Available at: http://doi.wiley.com/10.1029/2001JB000707.

Warren, C. & Aniya, M., 1999. The calving glaciers of southern South America. *Global and Planetary Change*, 22(1–4), pp.59–77.

www.dmi.dk, viewed 23.4.2019, https://www.dmi.dk/publikationer/.

www.knmi.nl, viewed 21.3.2019, https://climexp.knmi.nl/plot_atlas_form.py.

www.maps.greenmin.gl, viewed 23.3.2019, http://maps.greenmin.gl/geusmap/?mapname=greenland_portal&lang=en#baslay=baseMapGl&optlay=&extent=49517.73536506899,7771144.003588044,84875.74045768256,7789159.7490399955&layers=northpole_graticule,grl_geus_500k_geology_map.

www.maximintegrated.com, viewed 8.4.2019, https://www.maximintegrated.com/en/products/ibutton/data-loggers/DS1922L.html.

www.qgis.org, viewed 11.4.2019, https://www.qgis.org/de/site/.

www.regentinstruments.com, viewed 1.4.2019, https://www.regentinstruments.com/assets/products.html.

www.rinntech.de, viewed 8.4.2019, http://www.rinntech.de/content/view/17/48/lang,german/index.html.

www.sensefly.com, viewed 11.4.2019, https://www.sensefly.com/drone/ebee-mapping-drone/.

www.timeanddate.com, viewed 29.3.2019, https://www.timeanddate.com/sun/greenland/ilulissat.

www.youtube.com, viewed 19.4.2019, https://www.youtube.com/watch?v=2l5Da7fIKtI.

Zick, W., 1972. Eisbewegungen am Eqip Sermia und im westlichen Randgebiet des grönländischen Inlandeises (EGIG Arbeitsgebiet). *Polarforschung*, pp.24–30. Available at: http://epic.awi.de/27990/1/Polarforsch1972_1_4.pdf.

Zwally, H.J. et al., 2002. Surface Melt – Induced Acceleration of Greenland Ice-Sheet Flow. , 297(July), pp.218–222.

9 Appendix

Table 13: Single shrub information of every sampled shrub.

Single shrub information

Sample ID	Sampling Zone	Exposition	Vegetation Cover [%]	Height [cm]	Age [years]	Avg RW [µm]	Analysed sections	Missing rings	Elevation [m.a.s.l.]
B01_0a	0	NE	80	18	36	130.22	AS & SS	0	15.95
B04_0a	0	NNE	70	16	38	135.55	AS & SS	1	18.32
B05_0a	0	NNE	70	14	41	120.93	AS & SS	1	18.77
B06_0a	0	NNE	65	15	41	155.46	AS & SS	1	18.18
B08_0a	0	NNE	75	12	41	114.00	AS & SS	1	16.83
B09_0a	0	N	70	14	42	128.33	AS & SS	2	14.72
B10_0a	0	N	80	15	79	84.61	AS & SS	3	15.85
B13_0a	0	N	85	20	30	181.73	AS & SS	0	19.53
B14_0a	0	NE	95	17	22	206.18	AS & SS	0	16.52
B17_0a	0	N	85	22	66	90.53	AS & SS	0	19.21
B18_0a	0	NNE	80	12	41	138.02	AS & SS	0	18.84
B19_0a	0	NNW	70	19	28	155.68	AS & SS	0	19.05
B20_0a	0	NNW	70	24	52	173.27	AS & SS	0	20.12
Zone 0 avg		**NNE**	**76.54**	**16.77**	**42.85**	**139.58**		**0.69**	**17.84**
B41_1r	1	N	60	14	41	215.46	AS & SS	1	9.69
B42_1r	1	N	50	18	60	105.42	AS & SS	0	9.77
B43_1r	1	N	60	13	33	133.88	AS & SS	0	9.64
B44_1r	1	N	60	13	36	134.92	AS & SS	0	10.12
B45_1a	1	N	50	9	40	93.60	AS & SS	1	9.28
B46_1a	1	N	60	15	19	269.68	AS & SS	0	11.97
B47_1a	1	N	80	20	37	119.32	AS & SS	0	12.14
B48_1r	1	NE	65	11	21	185.00	AS & SS	1	12.25
B49_1a	1	N	45	15	28	190.71	AS & SS	0	11.85
B50_1a	1	NW	55	16	45	116.67	AS & SS	0	11.98
Zone 1 avg		**N**	**58.5**	**14.4**	**36**	**156.47**		**0.3**	**10.87**
B31_2d	2	NNE	10	11	33	111.30	AS & SS	1	11.98
B32_2r	2	NNE	15	13	35	119.94	AS & SS	0	12.02
B34_2d	2	NNE	15	9	27	217.81	AS & SS	0	11.43
B35_2r	2	N	5	13	32	99.38	AS & SS	2	9.03
B36_2r	2	N	10	9	25	135.64	AS & SS	2	8.95
B37_2r	2	N	30	10	36	133.06	AS & SS	2	8.78
B38_2d	2	N	20	14	49	144.61	AS & SS	0	9.13
B40_2r	2	N	5	14	23	170.61	AS & SS	1	8.81
Zone 2 avg		**N**	**13.75**	**11.63**	**32.50**	**141.54**		**1.00**	**10.02**
B21_3d	3	N	0	25	49	150.14	AS & SS	1	8.58
B22_3d	3	N	1	17	42	159.93	AS & SS	0	8.65
B24_3d	3	NNE	0	11	62	128.63	AS & SS	1	7.82
B26_3d	3	NNE	0	9	43	143.19	AS & SS	3	6.90
B27_3d	3	N	0	3	48	138.98	AS & SS	0	8.29
B28_3d	3	NNW	5	NA	51	141.00	AS & SS	2	8.33
B29_3d	3	NNW	0	NA	36	159.11	AS & SS	2	8.27
B51_3d	3	N	0	NA	34	182.50	AS & SS	1	8.79
Zone 3 avg		**N**	**0.75**	**13.00**	**45.63**	**150.44**		**1.25**	**8.21**

10 Acknowledgements

The completion of this master's thesis over the past year would not have been possible without the relentless help and support of the following people. First my gratitude goes out to my supervisors **Dr. Holger Gärtner** and **Prof. Dr. Andreas Vieli** who gave me the possibility to work on a unique and fascinating topic. Thank you for always having an open ear for my questions during all the steps taken over this time, sparking my interest in dendrogeomorphology and glaciology with your inspiring work and lectures at University of Zürich as well as the support before and during the fieldwork in Greenland. Further I would like to thank the following people:

- **Dr. Martin Lüthi** (GIUZ), for the organisation of the fieldwork in Greenland.
- **Simon Schudel** (GIUZ), for his assistance in the field.
- The technicians at WSL **Loïc Schneider** and **Anne Verstege** for all the help during the lab work and crossdating.
- **Fritz H. Schweingruber** (WSL), for lending me his book on Arctic vegetation, which made determination of plant species in the field a lot easier.
- **Dr. Christopher Sargeant** (WSL), for proofreading and all his valuable comments during the entire process – Thank you!
- **Dr. Guillaume Jouvet** (ETHZ), for providing drone images and a DEM of my study area.
- **Marius Vögtli** (GIUZ), for his help with QGIS.
- **Christoph Müller** and my sister **Andreina Manser**, for proofreading and valuable feedback.
- My parents **Gaby Inglin Manser & Roman Manser** for their immense support during my entire studies and for being there for me since I can remember.
- My fellow Master students of the **Y23-G-10 office** and the **WSL dendro group**, for mental and motivational support, distracting lunchbreaks and interesting discussions.

Finally, a special thanks goes out to the **Geographisch-Ethnographische Gesellschaft Zürich (GEGZ)** for their generous contributions towards my travel cost during the fieldwork in Greenland.

11 Personal Declaration

I hereby declare that the submitted thesis is the result of my own, independent work. All external sources are explicitly acknowledged in the thesis.

Zürich, 29th April 2019 Danijar Manser